

PREPARED FOR SUBMISSION TO JHEP

# What $R_K$ and $Q_5$ can tell us about New Physics in $b \rightarrow s\ell\ell$ transitions?

---

Marcel Algueró<sup>a</sup>, Bernat Capdevila<sup>a</sup>, Sébastien Descotes-Genon<sup>b</sup>, Pere Masjuan<sup>a</sup> and Joaquim Matias<sup>a</sup>

<sup>a</sup>*Universitat Autònoma de Barcelona, 08193 Bellaterra, Barcelona, Institut de Física d'Altes Energies (IFAE), The Barcelona Institute of Science and Technology, Campus UAB, 08193 Bellaterra (Barcelona).*

<sup>b</sup>*Laboratoire de Physique Théorique, UMR 8627, CNRS, Univ. Paris-Sud, Université Paris-Saclay, 91405 Orsay Cedex, France*

**ABSTRACT:** The deviations with respect to the Standard Model that are currently observed in  $b \rightarrow s\ell\ell$  transitions, or  $B$  anomalies, can be interpreted in terms of different New Physics (NP) scenarios within a model-independent effective approach. We identify a set of internal tensions of the fit that require further attention and whose theoretical or experimental nature could be determined with more data. In this landscape of NP, we discuss possible ways to discriminate among favoured NP hypotheses in the short term thanks to current and forthcoming observables. While the update of  $R_K$  will be an important milestone on the way to disentangle the type of NP we may be observing (Lepton-Flavour Universality Violating and/or Lepton Flavour Universal), additional observables, in particular  $Q_5$ , turn out to be central to determine which NP hypothesis should be preferred. We also analyse the preferences shown by the current global fit concerning various NP hypotheses, using two different tools: the behaviour of the pulls of individual observables under NP scenarios and the directions favoured by approximate quadratic parametrisations of the observables in terms of Wilson coefficients.

---

## Contents

<b>1</b>	<b>Introduction and motivation</b>	<b>1</b>
<b>2</b>	<b>Inner tensions of the global fit</b>	<b>4</b>
2.1	$R_{K^*}$ in the first bin	4
2.2	$B_s \rightarrow \phi \mu^+ \mu^-$ versus $B \rightarrow K^* \mu^+ \mu^-$	5
2.3	Tensions between large and low recoil in angular observables	6
<b>3</b>	<b>Potential of <math>R_K</math> (and <math>Q_5</math>) to disentangle NP hypotheses</b>	<b>8</b>
3.1	Global Fits	10
3.2	LFUV fits	14
<b>4</b>	<b>Pulls of individual observables</b>	<b>16</b>
4.1	Observables with a large $\text{pull}_i^{\text{obs}}$ within the Standard Model	17
4.2	Observables with no $\text{pull}_i^{\text{obs}}$ with respect to the Standard Model	20
<b>5</b>	<b>Sensitivity of observables to different Wilson coefficients</b>	<b>20</b>
5.1	Observables and parametrisations	21
5.2	Observables as conics	22
5.3	Directions favoured by the anomalies	24
<b>6</b>	<b>Conclusions</b>	<b>25</b>

---

## 1 Introduction and motivation

After the LHCb collaboration announced in April 2017 the measurement of the Lepton-Flavour Universality Violating (LFUV) observable  $R_{K^*}$ , the combined analysis of 175 LFUV and lepton-flavour dependent (LFD) observables performed in Ref. [1] using a model-independent approach showed that the Standard Model (SM) hypothesis is disfavoured compared to various hypotheses of New Physics (NP) contributions in  $b \rightarrow s \ell \ell$  decays, with pulls w.r.t. the SM ranging from  $5.3\sigma$  to  $5.8\sigma$ . Similar results were obtained by other groups using different treatments of hadronic uncertainties and sets of observables [2–10]. These model-independent analyses constrain NP scenarios expressed as contributions to the short-distance Wilson coefficients  $\mathcal{C}_{i\ell}$  in the effective Hamiltonian approach for  $b \rightarrow s \ell \ell$  transitions.

The first point to address is obviously whether NP has been discovered, but once this is established, it will prove important to determine the specific pattern of NP discovered. Indeed, even if the amount of data obtained up to now for  $b \rightarrow s \mu \mu$  makes sophisticated global fits to several Wilson coefficients possible [1–12], the outcome is still not conclusive

enough to draw definite conclusions about the actual pattern of NP. Disentangling the realized pattern is an essential guide to build NP models in agreement with these observations. It is therefore usual to limit NP contributions to a few Wilson coefficients, that from now on we will refer as hypotheses, and to build NP models in agreement with these assumptions of the global fits.

Most scenarios discussed in the literature assumed that there is NP in muons only, i.e. the LFUV-NP contributions come from allowing the presence of NP in the muon channel and not in the electron one (or it is considered small). Two particularly interesting scenarios have emerged, namely NP in  $\mathcal{C}_{9\mu}$  or in  $\mathcal{C}_{9\mu} = -\mathcal{C}_{10\mu}$ , with a larger significance for the first and a smaller one for the latter in Ref. [1]. On the contrary, we also found that a fit restricted to a subset of mainly LFUV observables (15 observables in total) exhibits a marginal preference for the  $\mathcal{C}_{9\mu}^{\text{NP}} = -\mathcal{C}_{10\mu}^{\text{NP}}$  scenario compared to  $\mathcal{C}_{9\mu}^{\text{NP}}$ . In addition, the best fit value of the scenario with NP only in  $\mathcal{C}_{9\mu}$  is rather different when considering all observables or the LFUV subset.

Recently, several works allowed for NP also in the electron channel, but no particular structure was envisaged from these fits by simply taking some of the electronic Wilson coefficients different from zero [8, 11, 13]. However, in a recent article [12], we allowed the possibility of a specific structure, namely, that the  $b \rightarrow s\ell\ell$  transitions get a common Lepton Flavour Universal (LFU) NP contribution for all charged leptons (electrons, muons and taus). This permitted us to identify new favoured NP hypotheses. This idea was implemented by allowing two NP contributions inside the semileptonic Wilson coefficients:

$$\mathcal{C}_{i\ell}^{\text{NP}} = \mathcal{C}_{i\ell}^{\text{V}} + \mathcal{C}_i^{\text{U}} \quad (1.1)$$

with  $\ell = e, \mu, \tau$  and where  $\mathcal{C}_{i\ell}^{\text{V}}$  stands for LFUV-NP and  $\mathcal{C}_i^{\text{U}}$  for LFU-NP contributions. We distinguished the two contributions by imposing that  $\mathcal{C}_{ie}^{\text{V}} = 0$ . It is important at this point to emphasize the difference between simply allowing the presence of NP also in electrons or allowing the existence of two different kinds of NP contributions (LFU and LFUV). The case of simply allowing NP in the electron channel has been discussed quite extensively in Ref. [13] (see also Ref. [8] for a smaller subset of scenarios and without including low-recoil observables). However, our approach of distinguishing LFU- and LFUV-NP structures provides new ideas to model building and extends the possible interpretations of the current fits. Performing the fits with this new setting, we obtained our previous results in Ref. [1] but also new scenarios different from Refs. [8, 13]. This can be seen by translating LFU and LFUV contributions into NP contributions to muons and electrons (leaving  $\tau$  aside at this stage)

$$\mathcal{C}_{9\mu}^{\text{NP}} = \mathcal{C}_{9\mu}^{\text{V}} + \mathcal{C}_9^{\text{U}}, \quad \mathcal{C}_{10\mu}^{\text{NP}} = \mathcal{C}_{10\mu}^{\text{V}} + \mathcal{C}_{10}^{\text{U}}, \quad \mathcal{C}_{9e}^{\text{NP}} = \mathcal{C}_9^{\text{U}}, \quad \mathcal{C}_{10e}^{\text{NP}} = \mathcal{C}_{10}^{\text{U}}. \quad (1.2)$$

This seemingly innocuous redefinition yields interesting consequences, as discussed in Ref. [12]. It opens interesting perspectives to explain with different mechanisms the anomalies coming purely from the muon sector (like  $\langle P_5' \rangle_{[4,6]}$ ) and the ones describing the violation of lepton flavour universality (like  $\langle R_K \rangle_{[1,6]}$ ). It may also explain the difference between the best fit point of the scenario  $\mathcal{C}_{9\mu}^{\text{NP}}$  in Ref. [1] if one considers all available observables or only LFUV observables, as the former will correspond to  $\mathcal{C}_{9\mu}^{\text{NP}}$  and the latter to  $\mathcal{C}_{9\mu}^{\text{V}}$ .

When translated from one language to the other, the most interesting scenarios in Ref. [12] become:

$$\begin{aligned}
& \{\mathcal{C}_{9\mu}^V = -\mathcal{C}_{10\mu}^V, \mathcal{C}_9^U, \mathcal{C}_{10}^U\} \rightarrow \{\mathcal{C}_{9\mu}^{\text{NP}} = -\mathcal{C}_{10\mu}^{\text{NP}} + 2\mathcal{C}_{9e}^{\text{NP}}, \mathcal{C}_{9e}^{\text{NP}}, \mathcal{C}_{10e}^{\text{NP}}\} \\
& \{\mathcal{C}_{9\mu}^V, \mathcal{C}_{10\mu}^V, \mathcal{C}_9^U = \mathcal{C}_{10}^U\} \rightarrow \{\mathcal{C}_{9\mu}^{\text{NP}}, \mathcal{C}_{10\mu}^{\text{NP}}, \mathcal{C}_{9e}^{\text{NP}} = \mathcal{C}_{10e}^{\text{NP}}\} \\
\text{[Hyp.V]} \quad & \{\mathcal{C}_{9\mu}^V = -\mathcal{C}_{10\mu}^V, \mathcal{C}_9^U = \mathcal{C}_{10}^U\} \rightarrow \{\mathcal{C}_{9\mu}^{\text{NP}} = -\mathcal{C}_{10\mu}^{\text{NP}} + 2\mathcal{C}_{9e}^{\text{NP}}, \mathcal{C}_{9e}^{\text{NP}} = \mathcal{C}_{10e}^{\text{NP}}\} \quad (1.3)
\end{aligned}$$

This additional NP component in  $b \rightarrow \text{see}$  explains the improved significance of the last scenario above (Hyp. V) compared to the favoured scenarios assuming NP in  $b \rightarrow s\mu\mu$  only in Ref. [1], which can be recast as:

$$\begin{aligned}
& \text{[Hyp. I]} \quad \{\mathcal{C}_{9\mu}^V\} \rightarrow \{\mathcal{C}_{9\mu}^{\text{NP}}\} \\
& \text{[Hyp. II]} \quad \{\mathcal{C}_{9\mu}^V = -\mathcal{C}_{10\mu}^V\} \rightarrow \{\mathcal{C}_{9\mu}^{\text{NP}} = -\mathcal{C}_{10\mu}^{\text{NP}}\} \quad (1.4)
\end{aligned}$$

Let us notice that this approach is also different from all the analyses including NP in electrons [8, 11, 13] where the muonic constrain  $\mathcal{C}_{9\mu} = -\mathcal{C}_{10\mu}$  does not receive any electronic contribution. For completeness, the remaining scenarios considered in Ref. [12] were:

$$\begin{aligned}
& \{\mathcal{C}_{9\mu}^V, \mathcal{C}_{10\mu}^V, \mathcal{C}_9^U, \mathcal{C}_{10}^U\} \rightarrow \{\mathcal{C}_{9\mu}^{\text{NP}}, \mathcal{C}_{10\mu}^{\text{NP}}, \mathcal{C}_{9e}^{\text{NP}}, \mathcal{C}_{10e}^{\text{NP}}\} \\
& \text{[Hyp.VI]} \quad \{\mathcal{C}_{9\mu}^V, \mathcal{C}_9^U\} \rightarrow \{\mathcal{C}_{9\mu}^{\text{NP}}, \mathcal{C}_{9e}^{\text{NP}}\} \\
& \text{[Hyp.VII]} \quad \{\mathcal{C}_{9\mu}^V = -\mathcal{C}_{10\mu}^V, \mathcal{C}_9^U\} \rightarrow \{\mathcal{C}_{9\mu}^{\text{NP}} = -\mathcal{C}_{10\mu}^{\text{NP}} + \mathcal{C}_{9e}^{\text{NP}}, \mathcal{C}_{10\mu}^{\text{NP}}, \mathcal{C}_{9e}^{\text{NP}}\} \quad (1.5)
\end{aligned}$$

We also introduce the additional scenario

$$\text{[Hyp. III]} \quad \{\mathcal{C}_{9\mu}^V = -\mathcal{C}_{9'\mu}^V\} \rightarrow \{\mathcal{C}_{9\mu}^{\text{NP}} = -\mathcal{C}_{9'\mu}^{\text{NP}}\} \quad (1.6)$$

and the LFUV two-dimensional scenario

$$\text{[Hyp. IV]} \quad \{\mathcal{C}_{9\mu}^V, \mathcal{C}_{10\mu}^V\} \rightarrow \{\mathcal{C}_{9\mu}^{\text{NP}}, \mathcal{C}_{10\mu}^{\text{NP}}\}. \quad (1.7)$$

We have named only a subset of scenarios for further reference, with hypotheses I to IV being purely LFUV NP and V to VII allowing both LFUV and LFU NP.

In this situation, it becomes clear that new data will be instrumental to disentangle the different hypotheses. The goal of the present article is to scrutinize the results of the fit from a different perspective to prepare the next step, i.e. to discriminate the most relevant NP scenario among the ones already favoured, complementing our two previous works, Refs. [1] and [14]. Currently, the most significant patterns identified exhibit a pull w.r.t the SM very close to each other (within a range of half a  $\sigma$ ). We explore strategies to disentangle different scenarios and to identify the impact of a precise measurement of  $R_K$ . We then combine information on  $R_K$  and  $Q_5$  in order to illustrate that  $R_K$  by itself will not be sufficient to disentangle clearly one or a small subset of scenarios, but that a combination of  $R_K$  and  $Q_5$  can be useful, depending on the (future) measured value <sup>1</sup>.

In section 2 we discuss the inner tensions of the fit in order to point those observables where further experimental or theoretical work would be required. In section 3 we explore

---

<sup>1</sup>Up to now only the Belle experiment has been able to perform a measurement of  $Q_5$ , leading to  $\langle Q_5^{\text{Belle}} \rangle_{[1,6]} = +0.656 \pm 0.485 \pm 0.103$  [15].

how a forthcoming precise measurement of  $R_K$  can disentangle or disfavour scenarios assuming that the statistical error is reduced and the central value stays within  $2\sigma$  of its present value. We analyse it considering two different fits, either with all observables or only the LFUV subset. We also discuss the impact of a measurement of  $Q_5$  in relation with its possible measurement by Belle II and LHCb. We then discuss the structure of the current fits, looking more closely at the deviations of some observables in section 4, focusing on the change in their pulls depending on the NP scenario considered. In section 5 we discuss the structure of the observables in terms of their Wilson coefficients to determine their sensitivities and the directions preferred by each of the anomalies, before drawing our conclusions.

## 2 Inner tensions of the global fit

In Ref. [1], we saw that different NP scenarios involving  $\mathcal{C}_{9\mu}^{\text{NP}}$  led to a much better description of the data than the SM, with fits reaching p-values around 60-70% (the SM being around 10%) and providing pulls with respect to the SM above  $5\sigma$ . The overall agreement is thus already very good within these NP scenarios and from a purely statistical point of view, it should be expected that these fits exhibit slight tensions. It is however interesting to look at these remaining tensions in more detail in order to determine where statistical fluctuations may be reduced with more data or where improved measurements might help to lift the degeneracy among NP scenarios. We focus on three main tensions that we consider particularly relevant in the current global fit.

### 2.1 $R_{K^*}$ in the first bin

A first tension related to  $R_{K^*}$  occurs in the global fit and it proves interesting to consider both  $R_{K^*}$  and  $\mathcal{B}(B \rightarrow K^*\mu^+\mu^-)$  in order to understand its nature (see Fig. 1).

Let us first consider the second bin (from 1 to 6  $\text{GeV}^2$ ) for  $R_{K^*}$ . Even though the deficit could be consistent with an excess in the electron channel with respect to the muon one, the study of the corresponding bins of  $\mathcal{B}(B \rightarrow K^*\mu^+\mu^-)$  points towards a deficit of muons. The mechanism that explains the deviation with respect to the SM in the long second bin of  $R_{K^*}$  is consistent with all the deviations that have been observed in other channels and different invariant di-lepton mass square regions.

The situation is different for the first bin of  $R_{K^*}$ , where the  $\mathcal{B}(B \rightarrow K^*\mu^+\mu^-)$  is clearly compatible with the SM (see Fig. 1). An excess in the electron channel would then be needed in order to explain the observed deficit in  $\langle R_{K^*} \rangle_{[1,1,6]}$ . This difference of mechanism between the first and the second bins of  $R_{K^*}$  can be understood in two ways: i) a specific NP effect [16] localised at very low  $q^2$  and able to compete with the dominant Wilson coefficient  $\mathcal{C}_7$  (well determined to be in agreement with the SM expectations from  $\mathcal{B}(B \rightarrow X_s\gamma)$ ) [1, 17–20]; ii) some experimental issue in measuring di-electron pairs at very small invariant mass, close to the photon pole. It would be very interesting that LHCb keep on their efforts to understand the systematics in this bin.

Another approach to slightly reduce the tension between data and SM in the first bin of  $R_{K^*}$  through a NP explanation consists in including NP contributions to the  $b \rightarrow see$

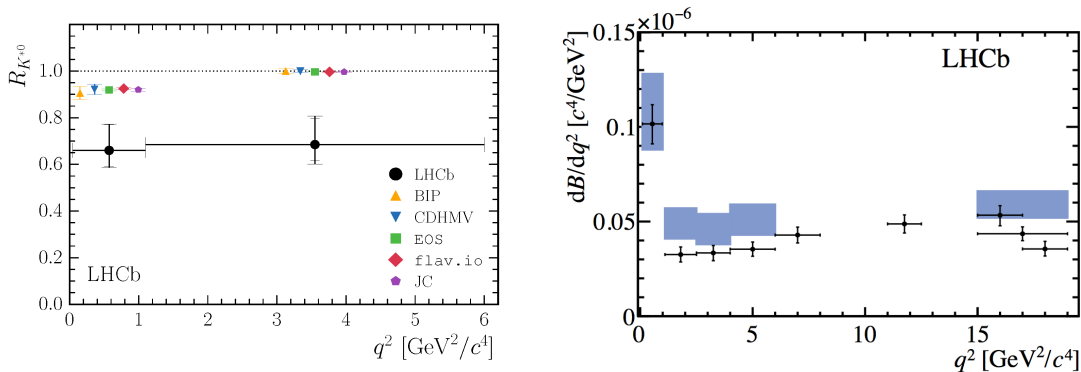


**Figure 1:**  $R_{K^*}$  (left panel) and  $\mathcal{B}(B \rightarrow K^* \mu^+ \mu^-)$  (right panel) measured by LHCb. Figures extracted from Refs. [21] and [22] respectively.

channel, in particular, considering right-handed currents affecting electrons, as discussed in Ref. [11]. In the scenarios S8-S11 (using the notation of Ref. [11]) the prediction of  $\langle R_{K^*} \rangle_{[0.045, 1.1]}$  is found to be within  $\sim 1\sigma$  range of the current measurement. This could open a new window to explore the existence of right-handed currents and to explain some of the tensions found, even though more data is required in order to be conclusive.

## 2.2 $B_s \rightarrow \phi \mu^+ \mu^-$ versus $B \rightarrow K^* \mu^+ \mu^-$

Another tension in the fit concerns the branching ratio for  $B_s \rightarrow \phi \mu^+ \mu^-$ , in particular when compared with the related decay  $B \rightarrow K^* \mu^+ \mu^-$ .

The prediction for the branching ratio  $\mathcal{B}(B \rightarrow K^* \mu^+ \mu^-)$  involves hadronic form factors to be determined using different theoretical approaches, depending on the di-lepton invariant mass region analysed: at large recoil, one can use light-cone sum-rules based on light-meson distribution amplitudes [23], while lattice form factors are available at low recoil. Due to the difficulty to assess precisely the uncertainties attached to light-cone sum rules, we perform our computation using more conservative results from light-cone sum rules based on  $B$ -meson distribution amplitudes [24] with conservative error estimates, exploiting QCD factorisation to restore correlations that were not available in Ref. [24]. We checked that our results are compatible with those obtained in Ref. [23] and that the two approaches yield very similar results for the fits [1–4].

A recent update of these form factors is available in Ref. [25] using the same approach as Ref. [24], adding corrections from higher twists and providing correlations. We will update our results accordingly in a coming publication, but we do not expect very significant changes for the present article, based on our previous studies [14]. For instance, we checked that even if a large reduction of 50% is achieved on the error of the form factors, the resulting uncertainty of key optimized observables like  $P'_5$  is minor (it would imply a reduction from 10% to 8% for the anomalous bins of  $P'_5$ ). On the contrary, a large impact is observed in unprotected observables like branching ratios or  $S_i$  observables. As our fit is driven by the optimized observables, we expect only minor changes in the outcome of the fits.

Contrary to the case of  $\mathcal{B}(B \rightarrow K^* \mu^+ \mu^-)$ , there are no computations available using the B-meson light-cone sum rules of Refs. [24, 25] for  $B_s \rightarrow \phi \mu^+ \mu^-$ , and one must rely on the estimates given in Ref. [23]. One can see in Fig. 2 that at low recoil, where lattice form factors are used, the prediction for  $\mathcal{B}(B \rightarrow K^* \mu^+ \mu^-)$  is expected to be slightly larger than  $\mathcal{B}(B_s \rightarrow \phi \mu^+ \mu^-)$  and indeed data (with large error bars) follows the same trend. On the contrary, in the large-recoil region where the light-cone sum rules results of Ref. [23] are used, the SM predictions lead to a larger value for  $\mathcal{B}(B_s \rightarrow \phi \mu^+ \mu^-)$  than for  $\mathcal{B}(B \rightarrow K^* \mu^+ \mu^-)$ . Surprisingly, data shows the opposite trend, which may come from a statistical fluctuation of the data leading to an inversion of the experimental measurements of both modes at large recoil. Alternatively, this issue may signal a problem in the theoretical prediction of the form factors of Ref. [23]. Firstly, these predictions are obtained by combining results in different kinematic regions (light-cone sum rules and lattice QCD) which do not fully agree with each other when they are extrapolated: the fit to a common parametrisation over the whole kinematic space leads to a fit with uncertainties that may be artificially small due to these incompatibilities of the inputs. Moreover, the choice of the  $z$ -parametrisation [23, 24] used to describe the form factors over the whole kinematic range has interesting properties of convergence, but it may in some cases lead to potential unitarity violations [27].

Finally, another issue that specifically affects  $\mathcal{B}(B_s \rightarrow \phi \mu^+ \mu^-)$  is the  $B_s$ - $\bar{B}_s$  mixing. As it is well known,  $B_s$ - $\bar{B}_s$  mixing implies that the time evolution of the  $B_s$  meson before its decay involves two mass states with different widths that are linear combinations of the flavour states  $B_s$  and  $\bar{B}_s$ . The current measurements performed at LHCb are integrated over time, and the neat effect of the evolution between the two mass states is a correction of  $O(\Delta\Gamma_s/\Gamma_s)$  in the relation between the theoretical computation of the branching ratio and its measurement [28–31]. This effect is taken into account in the global fit [2] as an additional source of uncertainty for the theoretical estimate of the branching ratios.

The experimental efficiencies should also be corrected for this effect, which depend on the CP-asymmetry  $A_{\Delta\Gamma}$  that can also be affected by NP contributions. It should thus be kept free within a large range in the absence of measurements. Neglecting this effect and assuming a SM value for this asymmetry may lead to an underestimation of some systematics on the efficiencies. For instance, Ref. [32] showed that this issue can lead to an additional systematic effect of 10% in the  $B_s \rightarrow \mu^+ \mu^-$  systematics. The impact on efficiencies from NP effects was indeed considered in Ref. [33] for  $B_s \rightarrow \phi \mu^+ \mu^-$  by varying  $\mathcal{C}_{9\mu}$  in the underlying physics model used to compute signal efficiencies, leading to a much smaller effect in this case (of a few percent, in line with back-of-the-envelope estimates).

### 2.3 Tensions between large and low recoil in angular observables

We discuss for the first time here a rather different type of tension, concerning the  $B \rightarrow K^* \mu^+ \mu^-$  angular observables at large and low recoil. On the one hand, we observe that branching ratios exhibit the same discrepancy pattern between theory and experiment at low and large recoil <sup>2</sup>. On the other hand, the current deviations at LHCb in  $P'_5$  require

---

<sup>2</sup>This is true for all  $b \rightarrow s\ell\ell$  modes, apart from the decay  $\Lambda_b^0 \rightarrow \Lambda \mu^+ \mu^-$ , where the experimental errors at low recoil are very large and the normalisation chosen prevents further interpretation [34, 35].

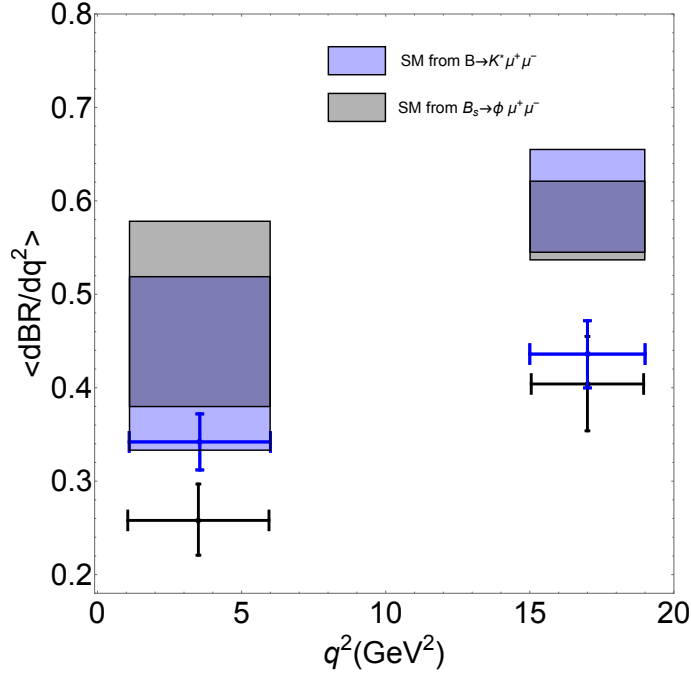


**Figure 2:** Theoretical predictions for  $\mathcal{B}(B_s \rightarrow \phi \mu^+ \mu^-)$  and  $\mathcal{B}(B \rightarrow K^* \mu^+ \mu^-)$  within the SM along with their corresponding experimental measurement. The results at large recoil are presented here only for illustrative purposes and are based on the form factors presented in Ref. [23] (these results are not used in our global analyses). The results at low recoil are indeed used in Ref. [2] and are based on available lattice QCD inputs for the form factors.

NP contributions with opposite sign in the two kinematic regions. Indeed, the pull between the SM value and the LHCb experimental measurement in  $\langle P'_5 \rangle_{[15,19]}$  has the opposite sign (albeit the significance is only  $1.2\sigma$ ) w.r.t. its large-recoil bins, in particular  $\langle P'_5 \rangle_{[4,6]}$  and  $\langle P'_5 \rangle_{[6,8]}$ . This very slight tension is not there in the case of the Belle data where same-sign deviations are observed, even though the error bars are rather large in this case.

For the purposes of illustration, let us consider the NP scenario where there is no LFU contribution and NP occurs only in  $\mathcal{C}_{9\mu}^V$  and  $\mathcal{C}_{10\mu}^V$ . This is illustrated in Fig. 3 where the constraints for these observables (as well as other relevant observables that will be listed below) are shown at 68.3% (left) and 95% (right) CL. One can notice their milder sensitivity to  $\mathcal{C}_{10\mu}^V$ .  $\langle P'_5 \rangle_{[4,6]}$  (blue region) would prefer a negative  $\mathcal{C}_{9\mu}^V$  while  $\langle P'_5 \rangle_{[15,19]}$  (green region) would favour a positive  $\mathcal{C}_{9\mu}^V$  at 68.3% CL.

Black dots indicate the particular solutions  $(-1.76, 0)$  and  $(-0.66, 0.66)$  corresponding to the best-fit points of the 1D favoured scenarios in Ref. [1] (hypotheses I and II of the present article). We also indicate the constraints from  $\langle P_2 \rangle_{[4,6]}$ ,  $\langle P_2 \rangle_{[15,19]}$ , and  $\langle R_K \rangle_{[1,6]}$ ,  $\langle \mathcal{B}(B^0 \rightarrow K^{*0} \mu^+ \mu^-) \rangle_{[15,19]}$  since we believe that they are representative of the set of observables driving our global fit<sup>3</sup>. The former pair of observables ( $\langle P_2 \rangle_{[4,6]}$ ,  $\langle P_2 \rangle_{[15,19]}$ ) has a large overlap region compatible with the SM while the latter one ( $\langle R_K \rangle_{[1,6]}$ ,

<sup>3</sup> $P_1$  and  $P'_4$  observables are known to behave in a more SM-like way than the ones selected here, thus

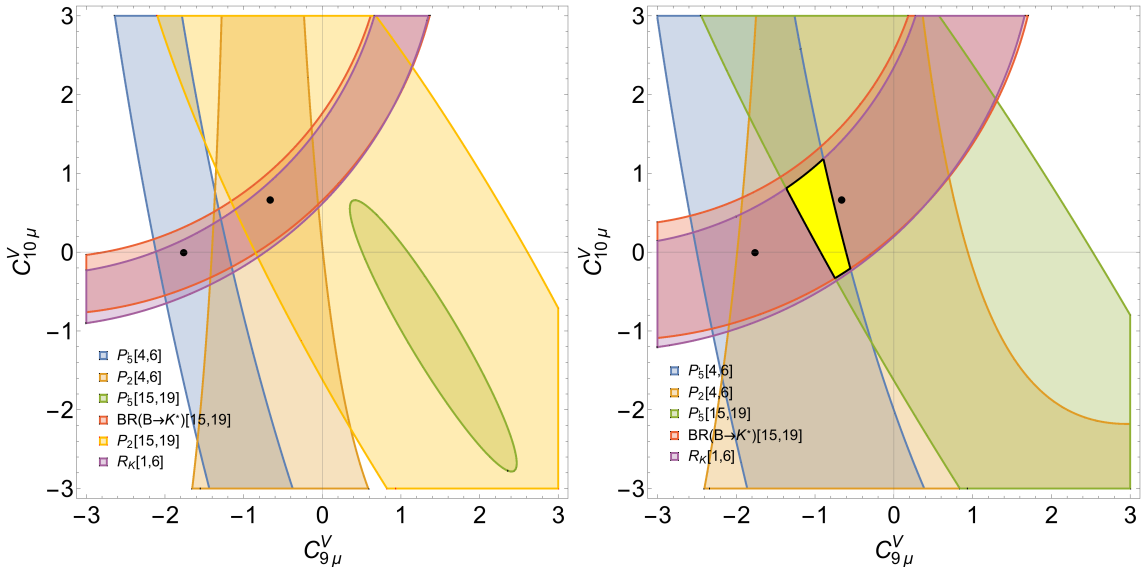


**Figure 3:** 68.3% (left) and 95% (right) CL solutions regions for the observables discussed in the main text in the  $(C_{9\mu}^V, C_{10\mu}^V)$  plane. The yellow region corresponds to the overlap region.  $\langle P_2 \rangle_{[15,19]}$  is only shown in the left panel.

$\langle \mathcal{B}(B^0 \rightarrow K^{*0} \mu^+ \mu^-) \rangle_{[15,19]}$  overlaps far from the SM point. While  $P_5'$  and  $R_K$  strongly constrain NP solutions, the  $P_2$  bins are weakly constraining. Finally, the yellow region in the right panel in Fig. 3 is the overlap of the regions from the five observables obtained after considering the data regions at 95% CL.

In summary, an interesting tension between low- and large-recoil regions for  $P_5'$  is observed at the 2-sigma level, favouring  $C_{9\mu}$  contributions of different signs in the two kinematic regions. Although not statistically significant, this inner tension seems to require either different sources of NP or a shift in the data once more statistics is added.

### 3 Potential of $R_K$ (and $Q_5$ ) to disentangle NP hypotheses

In this section we discuss the potential impact of the prospective measurements of  $\langle R_K \rangle_{[1,6]}$  and  $\langle Q_5 \rangle_{[1.1,6]}$  on the global fits in order to distinguish NP hypotheses. We perform the following illustrative exercise: we vary the experimental values of  $\langle R_K \rangle_{[1,6]}$  and  $\langle Q_5 \rangle_{[1.1,6]}$  within suitable ranges, and we perform fits according to these values taken as actual measurements. First only  $\langle R_K \rangle_{[1,6]}$  is allowed to vary before we consider the combined impact of  $\langle R_K \rangle_{[1,6]}$  and  $\langle Q_5 \rangle_{[1.1,6]}$ . The ‘pseudo-data’ for  $\langle R_K \rangle_{[1,6]}$  takes into account the increased statistics available for this observable, and we assume a reduced error by a factor 1.8 w.r.t. the present experimental statistical error following the prospects announced in Ref. [36]. Specifically for this exercise we take as the upper prospective experimental error for  $\langle R_K \rangle_{[1,6]}$   $+0.062$  and the lower error  $-0.055$ .

---

providing weaker constraints.

For each fit (corresponding to a given hypothesis and set of data), both the pull of the hypothesis w.r.t. the SM ( $\text{Pull}_{\text{SM}}$ ) and the best-fit-point (b.f.p) are computed, which we plot as functions of either  $\langle R_K \rangle_{[1,6]}$  or  $\langle Q_5 \rangle_{[1.1,6]}$ . Before discussing the results of our analysis, we first state our assumptions:

- ▶ We consider two different kind of fits with different subsets of observables [1]: on one side, the global fit (to all available observables) and on the other one, the LFUV fit, where only the observables measuring LFUV are included (plus constraints coming from radiative decays).
- ▶ Any variation of the experimental value of  $\langle R_K \rangle_{[1,6]}$  must manifest itself in a change in the branching ratios  $\mathcal{B}(B^+ \rightarrow K^+ \mu^+ \mu^-)$  and/or  $\mathcal{B}(B^+ \rightarrow K^+ e^+ e^-)$ . Here we should consider two different cases:
  - Global Fit: When we consider a fit to all observables, we must add a second assumption. Taking into account the fact that the observed systematic deficit in the muonic branching ratios *we assume that NP is purely of LFUV type and affects only muons and not electrons*. This means that varying the value of  $\langle R_K \rangle_{[1,6]}$  in the global fits should correspond also to a variation of the branching ratio  $\mathcal{B}(B^+ \rightarrow K^+ \mu^+ \mu^-)$  (whereas the electron mode is unaffected). This implies that for the global fits only scenarios measuring LFUV NP (hypotheses I to IV) can be considered in a consistent way.
  - LFUV Fit: On the contrary, the LFUV fits contain  $\langle R_K \rangle_{[1,6]}$  but no LFD branching ratios. We do not need to make any assumption on the changes in  $\mathcal{B}(B^+ \rightarrow K^+ e^+ e^-)$  and  $\mathcal{B}(B^+ \rightarrow K^+ \mu^+ \mu^-)$ , which opens the possibility of studying hypotheses with both LFU and LFUV NP contributions (hypotheses V to VII).
- ▶  $\langle R_K \rangle_{[1,6]}$  is freely varied within a  $2\sigma$  range from its current experimental value. It represents a good compromise between a high coverage of the true value and a span compatible with our computational means.  $\langle Q_5 \rangle_{[1.1,6]}$  is varied within the range  $[-0.1, 1.0]$  in order to ensure that we scan over values corresponding to the most relevant NP scenarios (see Fig. 2 of Ref. [12]).
- ▶ With the increased statistics available at Run 2, it will be possible for experiments to provide more precise determinations of key observables. Therefore, besides the reduction in the error of  $\langle R_K \rangle_{[1,6]}$  and the associated  $\mathcal{B}(B^+ \rightarrow K^+ \mu^+ \mu^-)$  observable (in some of the scenarios as discussed above), we assume a guesstimated uncertainty of order 0.1 for  $\langle Q_5 \rangle_{[1.1,6]}$ .

The purpose of this analysis is not to provide precise determinations of the pull of the SM and the b.f.p.s for different values of  $\langle R_K \rangle_{[1,6]}$  and  $\langle Q_5 \rangle_{[1.1,6]}$  but rather to gain qualitative knowledge on how experimental measurements of these two observables will drive the analyses. This is particularly true for the b.f.p. plots that will provide only the central value but not the confidence intervals obtained for the NP contributions.

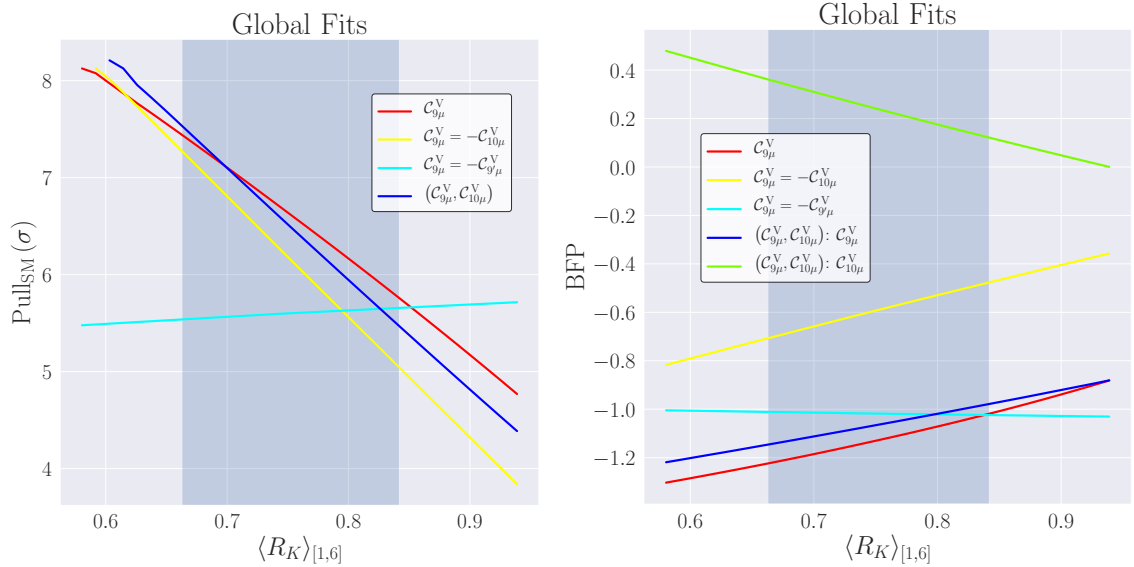


**Figure 4:** Impact of the central value of  $\langle R_K \rangle_{[1,6]}$  on the  $\text{Pull}_{\text{SM}}$  (left) and b.f.p.s (right) of the NP scenarios under consideration:  $\mathcal{C}_{9\mu}^V$  (red),  $\mathcal{C}_{9\mu}^V = -\mathcal{C}_{10\mu}^V$  (yellow),  $\mathcal{C}_{9\mu}^V = -\mathcal{C}_{9'\mu}^V$  (cyan) and  $(\mathcal{C}_{9\mu}^V, \mathcal{C}_{10\mu}^V)$  (blue). In the right panel colours are:  $\mathcal{C}_{9\mu}^V$  in  $(\mathcal{C}_{9\mu}^V, \mathcal{C}_{10\mu}^V)$  (blue) and  $\mathcal{C}_{10\mu}^V$  in  $(\mathcal{C}_{9\mu}^V, \mathcal{C}_{10\mu}^V)$  (green).

### 3.1 Global Fits

Figure 4 displays the outcome of the global fit with different experimental central values of  $\langle R_K \rangle_{[1,6]}$  under various NP hypotheses varied according to the procedure described above. The shaded vertical band in the plots of Figure 4 highlights the current experimental  $1\sigma$  confidence interval for  $\langle R_K \rangle_{[1,6]}$ .

The left panel in Figure 4 illustrates the relevance of  $\langle R_K \rangle_{[1,6]}$  on the global fits. For all the NP scenarios considered, except for  $\mathcal{C}_{9\mu}^V = -\mathcal{C}_{9'\mu}^V$ , we observe that their corresponding  $\text{Pull}_{\text{SM}}$  undergoes a  $\sim 4\sigma$  variation from one end of the range of variation to the other. If we restrict the variation of  $\langle R_K \rangle_{[1,6]}$  to only  $1\sigma$ , one can see differences of  $\sim 2\sigma$  between the two extremes, as expected from the linearity of  $\text{Pull}_{\text{SM}}$  on  $\langle R_K \rangle_{[1,6]}$  seen in the plots.

The flatness of the  $\text{Pull}_{\text{SM}}$  under the hypothesis  $\mathcal{C}_{9\mu}^V = -\mathcal{C}_{9'\mu}^V$  can be easily understood. The theoretical prediction of  $\langle R_K \rangle_{[1,6]}$  is insensitive to the value of  $\mathcal{C}_{9\mu}^V = -\mathcal{C}_{9'\mu}^V$ , so that it remains constant and equal to 1 to a very high accuracy. Therefore the difference between the theoretical and experimental values of  $\langle R_K \rangle_{[1,6]}$  does not play any role in the minimisation of the  $\chi^2$  function. As a consequence, the b.f.p. is determined using the other observables of the fit, regardless of the experimental value for  $\langle R_K \rangle_{[1,6]}$  (see the right-hand side plot of Fig. 4), and the contribution of  $\langle R_K \rangle_{[1,6]}$  cancels in the  $\Delta\chi^2 = \chi_{\text{SM}}^2 - \chi_{\text{min}}^2$  statistic. This explains the observed flat curve for the  $\text{Pull}_{\text{SM}}$ , up to small variations linked to the numerical minimisation of the  $\chi^2$  function.

The results in Figure 4 show that, for most of the values of  $\langle R_K \rangle_{[1,6]}$  scanned, it is not possible to fully disentangle all the NP scenarios, with the exception of  $\mathcal{C}_{9\mu}^V = -\mathcal{C}_{9'\mu}^V$ , but it

is possible to distinguish three regions:

- ▶  $0.58 \leq \langle R_K \rangle_{[1,6]} \lesssim 0.7$ : The NP scenarios  $\mathcal{C}_{9\mu}^V$ ,  $\mathcal{C}_{9\mu}^V = -\mathcal{C}_{10\mu}^V$  and  $(\mathcal{C}_{9\mu}^V, \mathcal{C}_{10\mu}^V)$  show similar pulls ( $\sim 7\sigma - 8\sigma$ ), where the 2D scenario stands out as the scenario with the highest preference over the SM. On the other hand,  $\mathcal{C}_{9\mu}^V = -\mathcal{C}_{9'\mu}^V$  sits at the  $5.5\sigma$  level, with a  $\sim 2.5\sigma$  difference with respect to the previous scenarios. Clearly, such small values for  $\langle R_K \rangle_{[1,6]}$  enhance the tensions between the SM and the experimental result, as reflected by the pulls and the b.f.p.s. which depart a lot from the SM.
- ▶  $0.7 \lesssim \langle R_K \rangle_{[1,6]} \lesssim 0.85$ : In this case, the new determination of  $\langle R_K \rangle_{[1,6]}$  is nominally close to its current experimental value (or slightly bigger) but with smaller errors. Therefore, the values for the b.f.p.s are numerically similar to the b.f.p.s reported in Ref. [1]. The pulls of the SM are all found between  $5.5\sigma$  and  $7\sigma$ , and we can only distinguish  $\mathcal{C}_{9\mu}^V = -\mathcal{C}_{9'\mu}^V$  from all the others except for values around  $\langle R_K \rangle_{[1,6]} \simeq 0.8$ . Among the three NP scenarios without right-handed coefficients,  $\mathcal{C}_{9\mu}^V$  is the one with the highest  $\text{Pull}_{\text{SM}}$  (all being around  $0.5\sigma$  of each other for most of this region).
- ▶  $0.85 \lesssim \langle R_K \rangle_{[1,6]} \leq 0.94$ : Here, most of the pulls decrease with respect to their present values, reaching between  $4\sigma$  and  $5.5\sigma$ . Even when  $\langle R_K \rangle_{[1,6]} \simeq 0.95$ , their significances get down to the range  $\sim 3.8\sigma - 4.8\sigma$ , apart from  $\mathcal{C}_{9\mu}^V = -\mathcal{C}_{9'\mu}^V$  that remains at  $\sim 5.5\sigma$ . Indeed, if a new measurement of  $\langle R_K \rangle_{[1,6]}$  is found in better agreement with its SM prediction, there is still an important number of other tensions (i.e.  $R_{K^*}$ ,  $P'_{5\mu}$  and  $\mathcal{B}(B_s \rightarrow \phi\mu^+\mu^-)$ ) that require NP contributions in order to be explained. Interestingly, this case may favour the hypothesis with right-handed currents  $\mathcal{C}_{9\mu}^V = -\mathcal{C}_{9'\mu}^V$  compared to other hypotheses.

Finally, we study the combined influence of  $\langle R_K \rangle_{[1,6]}$  and  $\langle Q_5 \rangle_{[1.1,6]}$ . The value of  $\langle Q_5 \rangle_{[1.1,6]}$  is varied as explained above and we repeat the analysis for three different values of  $\langle R_K \rangle_{[1,6]}$ : its current experimental value and the ends of its  $1\sigma$  range. In all cases, we work under the hypothesis of LFUV NP affecting only muons, namely, the experimental value of  $\mathcal{B}(B^+ \rightarrow K^+\mu^+\mu^-)$  and the associated error are modified as indicated at the beginning of this section. This implies that we restrict ourselves to hypotheses I to IV. The results are presented in Figs. 5 and 6. The first figure shows how the  $\text{Pull}_{\text{SM}}$  varies with different experimental values of  $\langle Q_5 \rangle_{[1.1,6]}$  and  $\langle R_K \rangle_{[1,6]}$  and the second shows how b.f.p.s are affected.

We observe that  $\mathcal{C}_{9\mu}^V = -\mathcal{C}_{10\mu}^V$  prefers small values of  $\langle Q_5 \rangle_{[1.1,6]}$ . For the hypotheses  $\mathcal{C}_{9\mu}^V$  and  $(\mathcal{C}_{9\mu}^V, \mathcal{C}_{10\mu}^V)$ , the bigger  $\langle Q_5 \rangle_{[1.1,6]}$  the greater the significance of the  $\text{Pull}_{\text{SM}}$  (as already observed in Fig. 2 of Ref. [12] and Fig. 6 of Ref. [1]). Except for  $\mathcal{C}_{9\mu}^V = -\mathcal{C}_{9'\mu}^V$ , increasing the value of  $\langle R_K \rangle_{[1,6]}$  amounts to shifting the  $\text{Pull}_{\text{SM}}$  curves to the right, although the shift size depends on the particular hypothesis. In addition, we extract the following conclusions:

- ▶  $\langle Q_5 \rangle_{[1.1,6]}$  is not able to distinguish between the three NP hypotheses:  $\mathcal{C}_{9\mu}^V$ ,  $\mathcal{C}_{9\mu}^V = -\mathcal{C}_{10\mu}^V$  and  $(\mathcal{C}_{9\mu}^V, \mathcal{C}_{10\mu}^V)$ , if the experimental value of  $\langle R_K \rangle_{[1,6]}$  is found to be  $1\sigma$  below its current determination. However, it is possible to discriminate between these three scenarios and  $\mathcal{C}_{9\mu}^V = -\mathcal{C}_{9'\mu}^V$ , since the latter has a lower  $\text{Pull}_{\text{SM}}$  by  $2\sigma$ .

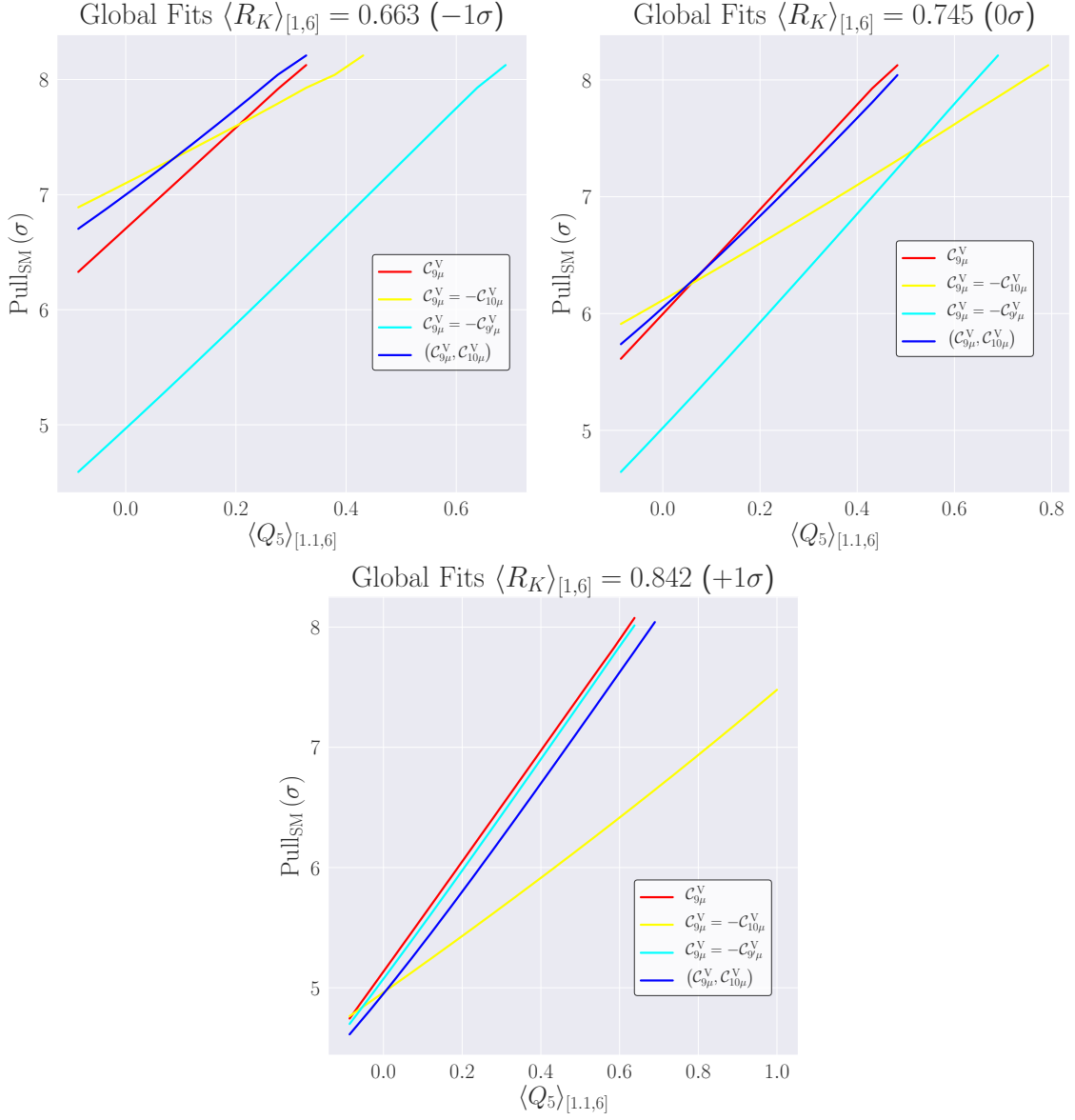


**Figure 5:** Impact of  $\langle Q_5 \rangle_{[1.1,6]}$  on the Pull<sub>SM</sub> of the NP scenarios under consideration for different values of  $\langle R_K \rangle_{[1,6]}$ . The following colour assignment is used:  $\mathcal{C}_{9\mu}^V$  (red),  $\mathcal{C}_{9\mu}^V = -\mathcal{C}_{10\mu}^V$  (yellow),  $\mathcal{C}_{9\mu}^V = -\mathcal{C}_{9\mu}^V$  (cyan) and  $(\mathcal{C}_{9\mu}^V, \mathcal{C}_{10\mu}^V)$  (blue).

- ▶ If  $\langle R_K \rangle_{[1,6]}$  stays at its current value and  $Q_5^{[1.1,6]} \gtrsim 0.4$ , then the measurement of  $\langle Q_5 \rangle_{[1.1,6]}$  allows one to disentangle  $\mathcal{C}_{9\mu}^V$  and  $(\mathcal{C}_{9\mu}^V, \mathcal{C}_{10\mu}^V)$  from  $\mathcal{C}_{9\mu}^V = -\mathcal{C}_{10\mu}^V$ . It is always possible to separate  $\mathcal{C}_{9\mu}^V = -\mathcal{C}_{9\mu}^V$  from the rest of scenarios except for  $0.4 \lesssim \langle Q_5 \rangle_{[1.1,6]} \lesssim 0.6$ .
- ▶ In the case where the central value of  $\langle R_K \rangle_{[1,6]}$  is increased by  $1\sigma$ ,  $\langle Q_5 \rangle_{[1.1,6]}$  is clearly able to disentangle  $\mathcal{C}_{9\mu}^V = -\mathcal{C}_{10\mu}^V$  from all the other scenarios if  $\langle Q_5 \rangle_{[1.1,6]} \gtrsim 0.2$ .

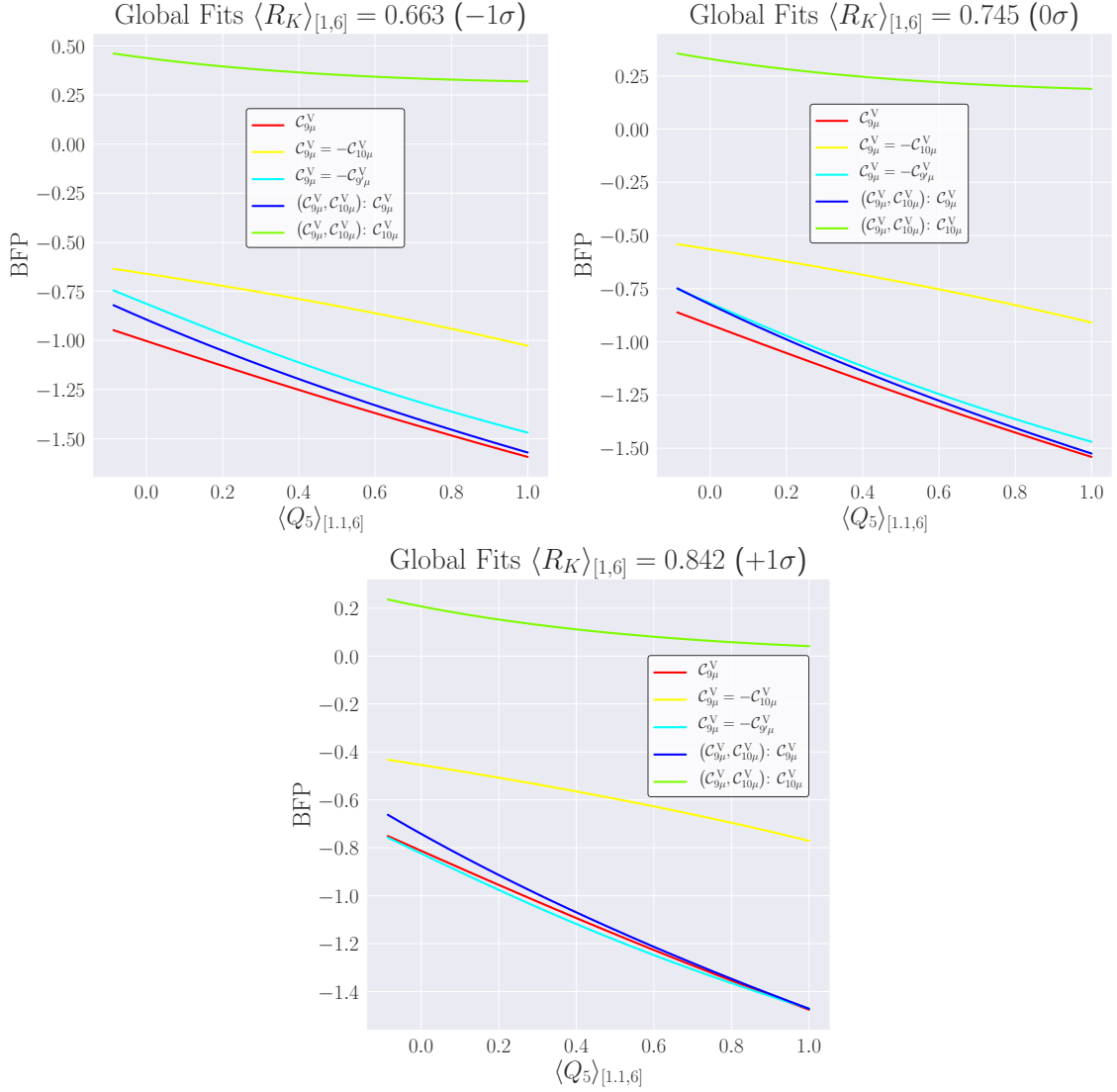


**Figure 6:** Impact of  $\langle Q_5 \rangle_{[1.1,6]}$  on the b.f.p.s of the NP hypotheses under consideration for different values of  $\langle R_K \rangle_{[1,6]}$ . The following colour assignment is used:  $\mathcal{C}_{9\mu}^V$  (red),  $\mathcal{C}_{9\mu}^V = -\mathcal{C}_{10\mu}^V$  (yellow),  $\mathcal{C}_{9\mu}^V = -\mathcal{C}_{9'\mu}^V$  (cyan),  $\mathcal{C}_{9\mu}^V$  in  $(\mathcal{C}_{9\mu}^V, \mathcal{C}_{10\mu}^V)$  (blue) and  $\mathcal{C}_{10\mu}^V$  in  $(\mathcal{C}_{9\mu}^V, \mathcal{C}_{10\mu}^V)$  (green).

Regarding the b.f.p.s (Fig. 6) and their behaviour with  $\langle Q_5 \rangle_{[1.1,6]}$ , we notice that the values of  $\mathcal{C}_{9\mu}^V$  for the scenarios  $\mathcal{C}_{9\mu}^V$ ,  $\mathcal{C}_{9\mu}^V = -\mathcal{C}_{9'\mu}^V$  and  $(\mathcal{C}_{9\mu}^V, \mathcal{C}_{10\mu}^V)$  tend to cluster together.

In summary, if the average between the new and old measurement of  $\langle R_K \rangle_{[1,6]}$  is below its current value, it would marginally increase the preference of the global fit for hypotheses with  $\mathcal{C}_{10\mu}^V$ , while a measurement above its Run-1 measurement would favour NP mainly in  $\mathcal{C}_{9\mu}^V$  or  $\mathcal{C}_{9\mu}^V = -\mathcal{C}_{9'\mu}^V$ . Values of  $\langle R_K \rangle_{[1,6]}$  below its Run-1 measurement would also clearly disfavour the hypothesis  $\mathcal{C}_{9\mu}^V = -\mathcal{C}_{9'\mu}^V$  with respect to the other three hypotheses. The observable  $\langle Q_5 \rangle_{[1.1,6]}$  is an excellent candidate to separate  $\mathcal{C}_{9\mu}^V = -\mathcal{C}_{10\mu}^V$  from  $\mathcal{C}_{9\mu}^V$ . In particular, values of  $\langle Q_5 \rangle_{[1.1,6]}$  bigger than 0.4 would disfavour the hypothesis  $\mathcal{C}_{9\mu}^V = -\mathcal{C}_{10\mu}^V$ .

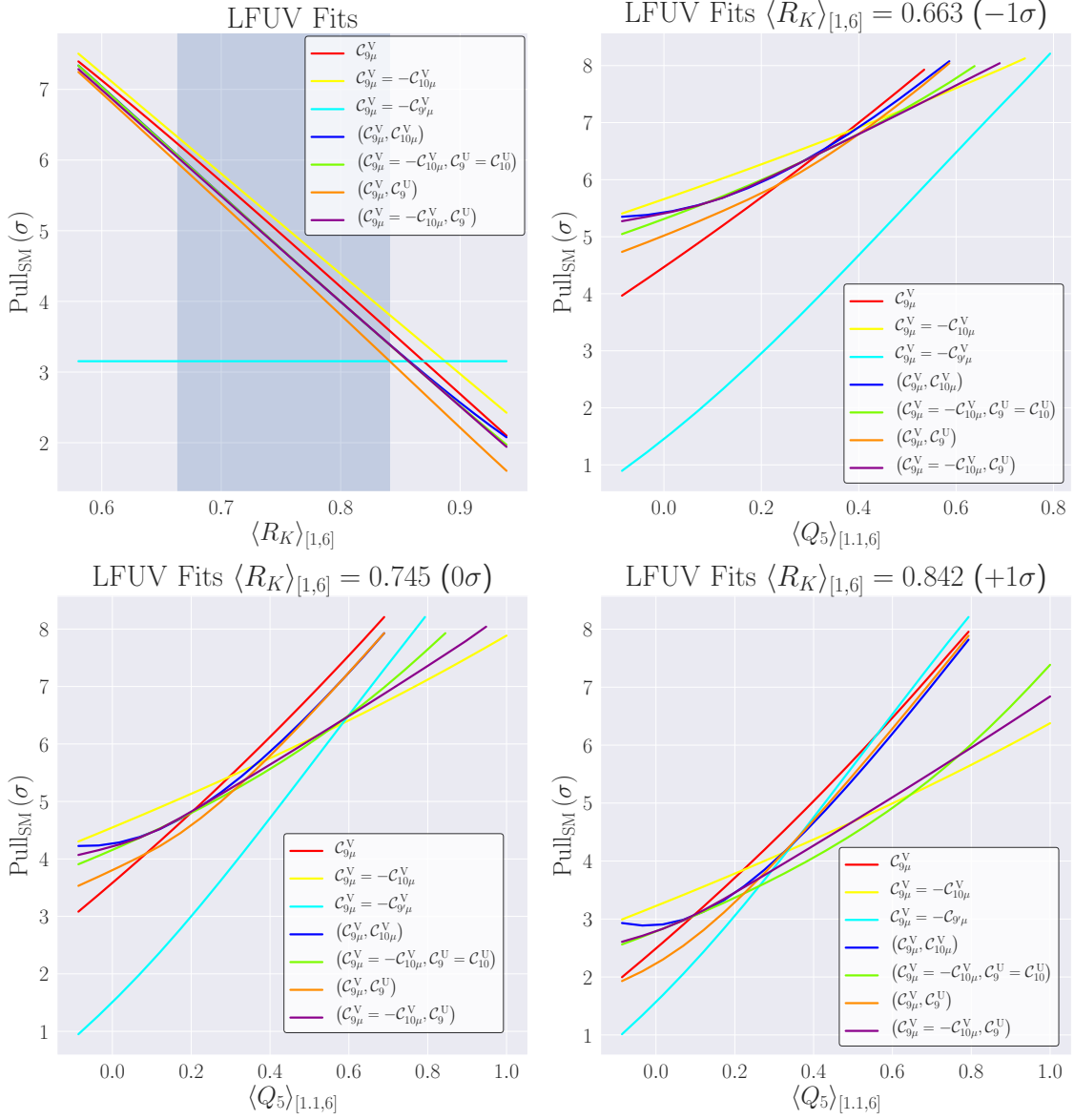


**Figure 7:** Impact of  $\langle R_K \rangle_{[1,6]}$  (top left) and  $\langle Q_5 \rangle_{[1,1,6]}$  for different values of  $\langle R_K \rangle_{[1,6]}$  (top right and bottom) on the Pull<sub>SM</sub> of the NP hypotheses under consideration. The following colour assignment is used:  $\mathcal{C}_{9\mu}^V$  (red),  $\mathcal{C}_{9\mu}^V = -\mathcal{C}_{10\mu}^V$  (orange),  $\mathcal{C}_{9\mu}^V = -\mathcal{C}_{9'\mu}^V$  (yellow),  $(\mathcal{C}_{9\mu}^V, \mathcal{C}_{10\mu}^V)$  (green),  $(\mathcal{C}_{9\mu}^V = -\mathcal{C}_{10\mu}^V, \mathcal{C}_9^U = \mathcal{C}_{10}^U)$  (cyan),  $(\mathcal{C}_{9\mu}^V, \mathcal{C}_9^U)$  (light blue) and  $(\mathcal{C}_{9\mu}^V = -\mathcal{C}_{10\mu}^V, \mathcal{C}_9^U)$  (dark blue).

compared to other hypotheses dominated by  $\mathcal{C}_{9\mu}^V$ .

### 3.2 LFUV fits

It is also interesting to address the impact of the observables  $\langle R_K \rangle_{[1,6]}$  and  $\langle Q_5 \rangle_{[1,1,6]}$  on the LFUV fits, which currently include  $R_K$  and  $R_{K^*}$  from LHCb, the measurements of

$Q_i$  ( $i = 4, 5$ ) by the Belle collaboration, all the  $b \rightarrow s\gamma$  observables available, as well as  $\mathcal{B}(B \rightarrow X_s\mu^+\mu^-)$  and  $\mathcal{B}(B_s \rightarrow \mu^+\mu^-)$  [37–39]. We follow the same guidelines as for the global fits, with the only difference that now hypotheses with LFU NP are also allowed.

Certain features are common in the two series of fits. For instance,  $\mathcal{C}_{9\mu}^V = -\mathcal{C}_{9'\mu}^V$  shows a constant behaviour and the linearity in the behaviour of the various pulls is still observed. Some remarks of this LFUV fit are in order:

- ▶ When analysing the impact of  $\langle R_K \rangle_{[1,6]}$  (top left panel in Fig. 7),  $\mathcal{C}_{9\mu}^V = -\mathcal{C}_{10\mu}^V$  is now the hypothesis with the most significant  $\text{Pull}_{\text{SM}}$  (though very close to the other ones that cluster together), contrary to the global fits that tend to prefer  $\mathcal{C}_{9\mu}^V$ . This was already observed in the LFUV fits performed in Ref. [1]: scenarios with  $\mathcal{C}_{9\mu}^V = -\mathcal{C}_{10\mu}^V$  are quite efficient in explaining  $R_K$  and  $R_{K^*}$  (see Fig. 5 of Ref. [1]). All hypotheses (apart from  $\mathcal{C}_{9\mu}^V = -\mathcal{C}_{9'\mu}^V$ ) yield pulls w.r.t. the SM with almost identical significance levels throughout the whole range of variation of  $\langle R_K \rangle_{[1,6]}$ , getting closer as  $\langle R_K \rangle_{[1,6]}$  deviates more and more from the SM. Hypotheses containing LFU NP are difficult to distinguish: in principle, LFUV observables contain cross terms that are products of LFU and LFUV NP contributions, but they are actually highly suppressed in all current LFUV observables. Let us add that the LFUV fits can yield pulls with very high significances at this level of precision in  $\langle R_K \rangle_{[1,6]}$ , moving from  $2\sigma$  to  $7\sigma$  when  $\langle R_K \rangle_{[1,6]}$  is varied.
- ▶ If we assume that the experimental value of the new average for  $\langle R_K \rangle_{[1,6]}$  is  $1\sigma$  below its present value and assess the impact of  $\langle Q_5 \rangle_{[1.1,6]}$  (top right panel in Fig. 7), we observe the same clear separation between the solution  $\mathcal{C}_{9\mu}^V = -\mathcal{C}_{9'\mu}^V$  and all the other hypotheses already pointed out in the context of global fits. For  $0.2 \lesssim \langle Q_5 \rangle_{[1.1,6]} \lesssim 0.5$ , it is not possible to identify a predominant hypothesis nor to distinguish between hypotheses (apart from  $\mathcal{C}_{9\mu}^V = -\mathcal{C}_{9'\mu}^V$ ). Small values of  $\langle Q_5 \rangle_{[1.1,6]}$  (close to zero or negative) favour  $(\mathcal{C}_{9\mu}^V, \mathcal{C}_{10\mu}^V)$  as well as hypotheses with  $\mathcal{C}_{9\mu}^V = -\mathcal{C}_{10\mu}^V$ .
- ▶ Keeping the central value of  $\langle R_K \rangle_{[1,6]}$  to its current value while scanning over  $\langle Q_5 \rangle_{[1.1,6]}$  (bottom left panel in Fig. 7), does not help in lifting the degeneracy in significance between the different hypotheses, specially for  $\langle Q_5 \rangle_{[1.1,6]} (\lesssim 0.4)$ . In this region  $\mathcal{C}_{9\mu}^V = -\mathcal{C}_{10\mu}^V$  is the preferred hypothesis but all of the pulls fall within less than  $1\sigma$ . However, for  $\langle Q_5 \rangle_{[1.1,6]} \gtrsim 0.4$ , it is indeed possible to classify the hypotheses in two groups: on the one side, preferred by the fit,  $\mathcal{C}_{9\mu}^V$ ,  $(\mathcal{C}_{9\mu}^V, \mathcal{C}_{10\mu}^V)$  and  $(\mathcal{C}_{9\mu}^V, \mathcal{C}_9^U)$  and, on the other side, all the other scenarios with  $\mathcal{C}_{9\mu}^V = -\mathcal{C}_{10\mu}^V$  which are disfavoured by the fit. In this case,  $\mathcal{C}_{9\mu}^V$  stands out as the scenario with the highest  $\text{Pull}_{\text{SM}}$ .
- ▶ Finally, we analyse the impact of  $\langle Q_5 \rangle_{[1.1,6]}$  assuming that the new average for  $\langle R_K \rangle_{[1,6]}$  lies  $1\sigma$  above its current determination (bottom right panel in Fig. 7). If  $\langle Q_5 \rangle_{[1.1,6]} \lesssim 0.3$ , there is no clear separation between hypotheses. On the contrary,  $\langle Q_5 \rangle_{[1.1,6]} \gtrsim 0.3$  separate the scenarios in two categories. On the one hand, all the scenarios where  $\mathcal{C}_{9\mu}^V$  is the dominant fit parameter cluster together, with significances between  $5\sigma$  and  $8\sigma$ . On the other hand, all the solutions with  $\mathcal{C}_{9\mu}^V = -\mathcal{C}_{10\mu}^V$  show lower significances

(by roughly  $1\sigma$ ). In this context,  $\mathcal{C}_{9\mu}^V = -\mathcal{C}_{9\mu}^V$  becomes the solution with the highest significance, although rather marginally.

In summary LFUV fits lead us to draw similar conclusions to the ones extracted from the global fits. However they exhibit a stronger clustering of the pulls, especially if only  $\langle R_K \rangle_{[1,6]}$  is used to discriminate them. Moreover, if we take a given hypothesis with LFUV-NP only, and consider hypotheses obtained by adding further LFU-NP contributions, we obtain very similar pulls. Therefore, the only way to distinguish among different LFU-NP hypotheses consists in performing the global fits and having access to both muonic and electronic branching ratios. The addition of  $\langle Q_5 \rangle_{[1.1,6]}$  allows for strategies that enable the discrimination of scenarios with a  $\mathcal{C}_{9\mu}^V = -\mathcal{C}_{10\mu}^V$  structure from scenarios with mainly NP in  $\mathcal{C}_{9\mu}^V$ , in a similar way to the case of the global fits.

#### 4 Pulls of individual observables

Discerning among different NP hypotheses using the significance of the  $\text{Pull}_{\text{SM}}$  proved difficult using the current set of data. In Sec. 3 we have discussed how new data could possibly improve the situation and allow us to disentangle the different scenarios. We discuss here a complementary approach based on analysing the current picture for each hypothesis using the correlated pull of individual observables.

We consider the *individual pull of an observable*, which can be written for the  $i^{\text{th}}$  observable as:

$$\text{pull}_i^{\text{obs}} = \sqrt{\chi_{\text{min}}^2 - \chi_{\text{min w/o obs } i}^2}, \quad (4.1)$$

where  $\chi_{\text{min}}^2$  and  $\chi_{\text{min w/o obs } i}^2$  are the minimal values of the  $\chi^2$  with and without the observables

$$\begin{aligned} \chi^2 &= \sum_{ij} (\mathcal{O}^{\text{th}} - \mathcal{O}^{\text{exp}})_i V_{ij}^{-1} (\mathcal{O}^{\text{th}} - \mathcal{O}^{\text{exp}})_j, \\ \chi_{\text{w/o obs } i}^2 &= \sum_{i \neq j} (\mathcal{O}^{\text{th}} - \mathcal{O}^{\text{exp}})_i V_{ij}^{-1} (\mathcal{O}^{\text{th}} - \mathcal{O}^{\text{exp}})_j, \end{aligned} \quad (4.2)$$

where  $\mathcal{O}^{\text{th}}$  and  $\mathcal{O}^{\text{exp}}$  are the theoretical prediction and the experimental value for the observable respectively, and  $V_{ij}^{-1}$  corresponds to the covariance matrix element  $\{i, j\}$ .

This definition, already used in Refs. [40–43], differs from the definition often adopted e.g. in the context of electroweak precision observables [44]: this naive pull is defined as the difference between the experimental value and the theoretical value at the b.f.p., normalised by the uncertainty. As discussed in Ref. [45], this definition should be refined. The pull of an observable can be considered as the assessment of the impact of the additional external constraint to the fit given by this observable, which must be assessed using a pull involving the central values and the uncertainties with and without the constraint given by the observable. It can be easily shown that the definition of Ref. [45] is equivalent to our definition. Moreover, this definition follows the same approach of pulls as for the comparison of hypotheses and it can be expected to follow a normal law with zero mean

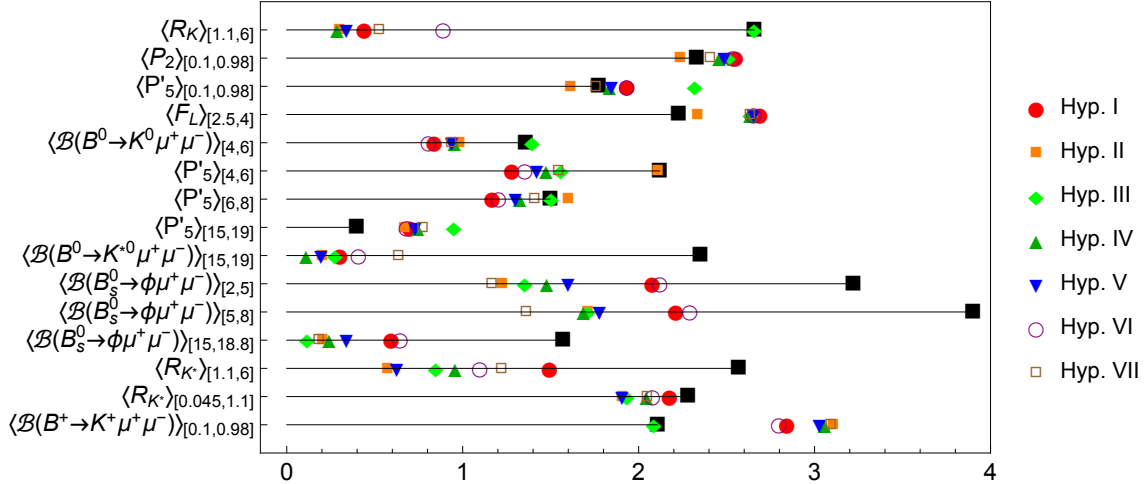


**Figure 8:** pull<sup>obs</sup> defined in Eq. (4.1) for each selected observable within different NP hypotheses (from I to VII) compared to the Standard Model (black squares).

and unit width. We stress that it includes correlations, so that it might have a different value from the naive pull in the presence of large correlations among observables (from experimental or theoretical nature).

In the following, we will compare the pulls of observables defined in Eq. (4.1) under the SM hypothesis and under the various NP hypotheses (I to VII) for all observables. However, we will focus mainly on the observables yielding pulls<sup>obs</sup> larger than 1.5. These pulls<sup>obs</sup> with respect to the SM are expected to be reduced under the various NP hypotheses, but some might remain (while the others disappear), providing interesting insights into the role of the various observables within a given NP hypothesis.

The observables under discussion are visualized in Fig. 8. In this figure, black squares represent the pull<sup>obs</sup> of the observable  $i$  within the SM computed following Eq. (4.1), while coloured and empty shapes represent the pull<sup>obs</sup> of the same observable under different NP hypotheses.

#### 4.1 Observables with a large pull <sub>$i$</sub> <sup>obs</sup> within the Standard Model

Looking at Fig. 8, the first observable considered is  $\langle R_K \rangle_{[1,6]}$ : it is very sensitive to LFUV NP, it has a large pull<sup>obs</sup> with respect to the SM and it should be updated very soon. It has also a small pull<sup>obs</sup> in all the NP hypotheses considered except for Hyp. III. Remarkably, it has almost no correlation with any other observable in the fit<sup>4</sup> [46] and, as a consequence, the fit must satisfy both  $\langle R_K \rangle_{[1,6]}$  and the rest of the observables in parallel, leading to a potential tension unless the solution for both sectors of the fit is similar. It turns out

<sup>4</sup>There is little theoretical correlation between  $R_K$  and the rest of the observables as the hadronic form factors, which are the main source of correlated uncertainty among observables, cancel in  $R_K$ . The experimental correlation between  $R_K$  and the  $B^+ \rightarrow K^+ \ell \ell$  branching ratio is not public and therefore assumed to be zero here. We checked the lack of correlation between  $\langle R_K \rangle_{[1,6]}$  and the rest of the observables at the level of our covariance matrix.

that for our favoured hypotheses, the b.f.p. for the global fit is well compatible with the current  $\langle R_K \rangle_{[1,6]}$  value. Let us consider for instance the hypotheses I and II, i.e.  $\mathcal{C}_{9\mu}^{\text{NP}}$  and  $\mathcal{C}_{9\mu}^{\text{NP}} = -\mathcal{C}_{10\mu}^{\text{NP}}$ . We can determine the value of the NP contribution needed to have the theoretical value of  $\langle R_K \rangle_{[1,6]}$  match its experimental value exactly. We can then compute the value of the  $\chi^2$  for the global fit for this particular value of the NP contribution. Comparing this value of the  $\chi^2$  with the  $\chi_{\text{min}}^2$  obtained after fitting all observables (including  $\langle R_K \rangle_{[1,6]}$ ), we observe that that the difference is 3 units for Hyp. I and 0.1 units for Hyp. II. This shows a good consistency between the current values of  $\langle R_K \rangle_{[1,6]}$  and the rest of the observables. If we perform the same exercise taking an experimental value of  $\langle R_K \rangle_{[1,6]}$  that would be  $1\sigma$  larger, the difference between  $\chi^2$  and  $\chi_{\text{min}}^2$  is  $\sim 2$  in both Hyp. I and II, so that these scenarios could still explain all deviations in a consistent way. Contrarily, if  $\langle R_K \rangle_{[1,6]}$  is lower by  $1\sigma$ , Hyp. I would display  $\chi^2 - \chi_{\text{min}}^2 \sim 30$  whereas Hyp. II would remain basically unchanged, indicating that the latter would show a better ability to explain  $R_K$  and the rest of the data.

Another observable showing a tension with the SM is  $\langle P_2 \rangle_{[0.1,0.98]}$ . Remarkably, none of the hypotheses considered is able to reduce the tension of this observable (see Fig. 8) so it remains poorly explained either within the SM or under the NP hypotheses considered. Even when we vary the central values for  $\langle R_K \rangle_{[1,6]}$  and  $\mathcal{B}(B^+ \rightarrow K^+ \mu^+ \mu^-)$ , this observable cannot be easily accommodated. Under some of our NP hypotheses, its  $\text{pull}^{\text{obs}}$  is slightly worse than within the SM. A similar problem is seen in  $\langle P_5' \rangle_{[0.1,0.98]}$  even though for this observable the  $\text{pull}^{\text{obs}}$  within the SM is smaller than for  $\langle P_2 \rangle_{[0.1,0.98]}$ . Including a NP contribution to  $\mathcal{C}_7$  (which affects mainly the first bin) does not improve these two observables as they require contributions of opposite signs. Therefore, the small tensions observed in the first bin for these two observables will require more data to be understood.

The polarization fraction  $\langle F_L \rangle_{[2.5,4]}$  follows a similar trend as  $\langle P_5' \rangle_{[0.1,0.98]}$ . Its current measurement shows little deviation with the SM prediction [2] in any of its bins due to the large theoretical errors, but its  $\text{pull}^{\text{obs}}$  is around  $\sim 2$  under the SM hypothesis due to the correlations with the rest of the observables involved in the fit. Moreover, for all NP hypotheses considered its value for the  $\text{pull}^{\text{obs}}$  is larger than in the SM case. Let us add that if we increase by  $1\sigma$  the central values for the observables  $\langle R_K \rangle_{[1,6]}$  and  $B^+ \rightarrow K^+ \mu^+ \mu^-$  branching ratio, the  $\text{pull}^{\text{obs}}$  for  $\langle F_L \rangle_{[2.5,4]}$  gets reduced.

In the case of the observables  $\langle P_5' \rangle_{[4,6]}$  and  $\langle P_5' \rangle_{[6,8]}$  the tension between the SM prediction and the experimental value is somewhat reduced if one introduces NP contributions. The less efficient hypothesis is Hyp. II,  $\mathcal{C}_{9\mu}^{\text{NP}} = -\mathcal{C}_{10\mu}^{\text{NP}}$ , and the best one is Hyp. I, i.e. a single contribution  $\mathcal{C}_{9\mu}^{\text{NP}}$ . As shown in Fig. 9, this hypothesis (grey band) would help accommodating at the same time both the deviations in  $\langle P_5' \rangle_{[4,6]}$  and  $\langle R_K \rangle_{[1,6]}$ . If  $\langle R_K \rangle_{[1,6]}$  were  $1\sigma$  larger than the current measurement, Hyp. I would still be favoured compared to the other hypotheses considered. The large value of  $\langle P_5' \rangle_{[4,6]}$  could be explained thanks to a LFU contribution  $\mathcal{C}_9^{\text{U}} = \mathcal{C}_{10}^{\text{U}}$  [12] (corresponding to Hyp. V), since  $\langle R_K \rangle_{[1,6]} = 1 + 0.49\mathcal{C}_{9\mu}^{\text{V}}$  while  $\langle P_5' \rangle_{[4,6]} = -0.81 - 0.27\mathcal{C}_9^{\text{U}} - 0.14\mathcal{C}_{9\mu}^{\text{V}} + 0.07(\mathcal{C}_9^{\text{U}})^2 + 0.05(\mathcal{C}_{9\mu}^{\text{V}})^2 + 0.11\mathcal{C}_9^{\text{U}}\mathcal{C}_{9\mu}^{\text{V}}$  [12]. This implies that a NP scenario with  $\mathcal{C}_{9\mu}^{\text{V}} = -\mathcal{C}_{10\mu}^{\text{V}}$  would then need a LFU universal contribution  $\mathcal{C}_9^{\text{U}} = \mathcal{C}_{10}^{\text{U}}$  to be viable. This is illustrated in Fig. 9 where Hyp. V is displayed varying the LFU contribution within its  $1\sigma$  confidence interval according to the global fit. As can be

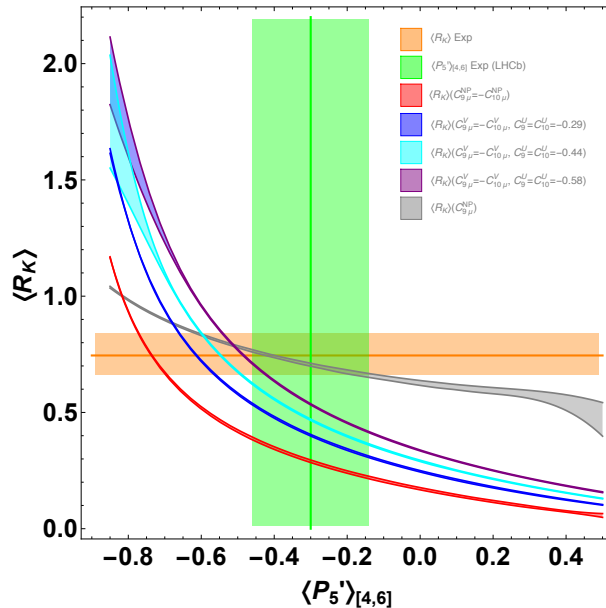


**Figure 9:**  $\langle R_K \rangle_{[1,6]}$  versus  $\langle P_5' \rangle_{[4,6]}$  in three different scenarios:  $C_{9\mu}^V$  (grey),  $C_{9\mu}^V = -C_{10\mu}^V$  (red), and  $C_{9\mu}^U = -C_{10\mu}^U$ ,  $C_9^U = C_{10}^U$  (three different values of the LFU contributions, blue, light blue and purple). In each case, the band is obtained by varying the LFU contribution within  $1\sigma$ . The current experimental values from LHCb are also indicated (green vertical and orange horizontal bands).

seen, if  $\langle R_K \rangle_{[1,6]}$  were  $1\sigma$  larger than the current measurement, Hyp. V would need an even bigger value (in module) for  $C_9^U = C_{10}^U$  than the  $1\sigma$  variation that we show in Fig. 9.

One of the tensions of the fits described in Sec. 2.3 belongs to the low-recoil region. This corresponds mainly to two observables here:  $\langle P_5' \rangle_{[15,19]}$  and  $\langle \mathcal{B}(B^0 \rightarrow K^{*0} \mu^+ \mu^-) \rangle_{[15,19]}$ . For  $\langle P_5' \rangle_{[15,19]}$ , including NP contributions leads to an increase of  $\text{pull}^{\text{obs}}$  in all cases, see Fig. 8. The reduction of this tension would require NP contributions of opposite sign to the ones favoured by the rest of the observables of the fit. On the other hand, the branching ratio  $\langle \mathcal{B}(B^0 \rightarrow K^{*0} \mu^+ \mu^-) \rangle_{[15,19]}$  has its  $\text{pull}^{\text{obs}}$  reduced under all NP hypotheses. This shows that the correlations between  $\langle \mathcal{B}(B^0 \rightarrow K^{*0} \mu^+ \mu^-) \rangle_{[15,19]}$  and the rest of the observables allow for the reduction of tensions provided under the different favoured NP hypotheses.

Deviations with respect to the SM are also found for the branching ratio of the  $B_s \rightarrow \phi \mu^+ \mu^-$  channel. All NP hypotheses yield  $\text{pulls}^{\text{obs}}$  smaller than their SM counterparts, specially for the low-recoil bin and parallel to its  $B \rightarrow K^*$  counterpart. The preferred scenarios considering the three bins of the branching ratio in the  $B_s \rightarrow \phi \mu^+ \mu^-$  channel from Fig. 8 are those with  $C_{9\mu}^V = -C_{10\mu}^V$ .

Finally, the tension for  $\langle R_{K^*} \rangle_{[1,1,6]}$  is also alleviated by introducing a NP contribution. In this case the most efficient is Hyp. II, while Hyp. I is clearly the worst. Whereas the large bin  $\langle R_{K^*} \rangle_{[1,1,6]}$  gets a significant reduction in its  $\text{pull}^{\text{obs}}$  under all NP hypotheses, the first bin  $[0.1, 0.98]$  is just slightly improved when compared to the SM. This could point towards

an inconsistency between the first bin and the other bins of  $R_{K^*}$  if one takes into account the issues discussed above regarding the first bin of  $P_2$  and  $P_5'$ . We should comment here on Ref. [11], where several NP scenarios are discussed in order to explain the low value of  $\langle R_{K^*} \rangle_{[0.1,0.98]}$ , including contributions to both  $b \rightarrow s\mu\mu$  and  $b \rightarrow see$  channels as well as considering the presence of right-handed currents. It is possible to connect some of the scenarios from [11] with the description of NP in terms of LFU and LFUV contributions proposed in Ref. [12]. Remarkably, the Wilson coefficients obtained in scenario S10 of [11] (following their notation) are in excellent agreement with the results obtained in [12] for the 4D fit with  $\{\mathcal{C}_{9\mu}^V, \mathcal{C}_{10\mu}^V, \mathcal{C}_9^U, \mathcal{C}_{10}^U\}$ .

Hyp. II works slightly better than Hyp. I in reducing the  $\text{pull}^{\text{obs}}$  of the LFUV observables, as can be easily understood looking at the structure of the observables in terms of their Wilson coefficients provided in Ref. [12]:  $\langle R_K \rangle_{[1,6]} = 1 + 0.23\mathcal{C}_{9\mu}^V - 0.26\mathcal{C}_{10\mu}^V$  while  $\langle R_{K^*} \rangle_{[1.1,6]} = 1 + 0.16\mathcal{C}_{9\mu}^V - 0.29\mathcal{C}_{10\mu}^V$ . Then, the ratio  $(\langle R_K \rangle_{[1,6]} - 1)/(\langle R_{K^*} \rangle_{[1.1,6]} - 1)$  turns out to be 1.4 in Hyp. I and 1.1 in Hyp. II. Experimentally, the ratio is basically 0.9, closer to the value given by Hyp. II (although Hyp. I is favoured in order to explain  $B \rightarrow K^* \mu^+ \mu^-$  angular observables). If  $\langle R_K \rangle_{[1,6]}$  and  $\mathcal{B}(B^+ \rightarrow K^+ \mu^+ \mu^-)$  had central values  $1\sigma$  higher than their actual experimental value, i.e. closer to the SM value, Hyp. I would also be favoured.

## 4.2 Observables with no $\text{pull}_i^{\text{obs}}$ with respect to the Standard Model

The kind of analysis undertaken in the previous subsection can also be conducted starting from observables that currently have very small  $\text{pulls}^{\text{obs}}$  with respect to the SM predictions and see how they are affected once a fit under a NP hypothesis is performed. It is to expect their  $\text{pulls}^{\text{obs}}$  will grow under NP hypotheses unless they are observables insensitive to the NP hypotheses considered. For this purpose we consider a group of observables with pulls between 0 and 0.2 within the SM.

After a detailed analysis, we found very small  $\text{pulls}^{\text{obs}}$  for all of them, except  $\langle \mathcal{B}(B^+ \rightarrow K^+ \mu^+ \mu^-) \rangle_{[0.1,0.98]}$ , under all the NP hypotheses considered, i.e. they are basically NP insensitive. In other words, these observables could be removed from the fit and the rest of the observables would remain unaffected. It is remarkable that again an observable taken in the first bin,  $\langle \mathcal{B}(B^+ \rightarrow K^+ \mu^+ \mu^-) \rangle_{[0.1,0.98]}$ , has a worse  $\text{pull}^{\text{obs}}$  under all NP hypotheses than under the SM. This goes in the same direction as the issues observed in the first bin of observables of the  $B \rightarrow K^* \mu^+ \mu^-$  channel such as  $P_2$ ,  $P_5'$  and  $R_{K^*}$ , which points out the need of a better understanding of the low- $q^2$  region.

## 5 Sensitivity of observables to different Wilson coefficients

A detailed scrutiny of the dependence in Wilson coefficients of  $b \rightarrow s\ell\ell$  observables is useful in order to understand tensions in the global fit under various NP hypotheses. The complexity of the calculation prevents such systematic study, but we will rely on an approximate parametrisation of the observables in order to identify the sensitivity of interesting observables to different Wilson coefficients/NP hypotheses.

## 5.1 Observables and parametrisations

We use our current programs [2] to generate predictions according to a grid in the space of Wilson parameters and fit the proposed parametrisations to this set of pseudo-data. We collect the coefficients in the vector

$$X = \{\mathcal{C}_{9\mu}^{\text{NP}}, \mathcal{C}_{10\mu}^{\text{NP}}, \mathcal{C}_{9'\mu}, \mathcal{C}_{10'\mu}, \mathcal{C}_{9e}^{\text{NP}}, \mathcal{C}_{10e}^{\text{NP}}, \mathcal{C}_{9'e}, \mathcal{C}_{10'e}\} \quad (5.1)$$

For simplicity, we consider only real NP contributions to the Wilson coefficients  $\mathcal{C}_{9,9',10,10'}$  for muon and for electron operators: we assume that we can neglect NP contributions to  $\mathcal{C}_7, \mathcal{C}_{7'}$  (based on  $b \rightarrow s\gamma$  observables in good agreement with the SM) as well as to scalar, pseudoscalar and tensor operators (based on the outcome of the general global fits performed on  $b \rightarrow s\ell\ell$  observables which do not favour large contributions to these Wilson coefficients. We also neglect imaginary contributions for the Wilson coefficients (as there are no signals of NP sources of CP violation from the corresponding  $b \rightarrow s\ell\ell$  observables). We consider only the set of LHCb observables present in the global fit of Ref. [2] with the corresponding binning in  $q^2$ , as well as the Belle observables  $Q_4$  and  $Q_5$ . We generate points along a grid for all  $\mathcal{C}_{i\ell}^{\text{NP}}$  ( $\ell = \mu, e$ ) in the range  $[-1, 1]$  for  $i = 10, 9', 10'$ , but  $[-2, 0]$  for  $i = 9$ , computing both central values and theoretical uncertainties for all the observables of interest. We can divide the set of observables into three different groups: LFD observables, LFUV differences and LFUV ratios, with three different approximate quadratic parametrisations:

- LFD observables: this category includes branching ratios and (optimized and averaged) angular observables [47, 48] governed by a lepton-specific  $b \rightarrow s\ell\ell$  transition. We use a general quadratic parametrisation in the NP contributions to the Wilson coefficients ( $i, j = 9, 10, 9', 10'$ ):

$$\mathcal{O} = \alpha + \sum_i \beta_i \mathcal{C}_{i\ell}^{\text{NP}} + \sum_{i \geq j} \gamma_{ij} \mathcal{C}_{i\ell}^{\text{NP}} \mathcal{C}_{j\ell}^{\text{NP}} \quad (5.2)$$

- LFUV differences:  $Q_{1,2,4,5}$  and  $\delta S_{5,6s}$  observables that measure differences in angular observables between muonic and electronic channels [49],

$$Q_i = P_{i\mu}^{(\prime)} - P_{ie}^{(\prime)}, \quad \delta S_i = S_{i\mu} - S_{ie} \quad (5.3)$$

In this case we use the following parametrisation ( $i, j = 9, 10, 9', 10'$ )

$$\begin{aligned} \mathcal{O}_\mu - \mathcal{O}_e &= \alpha_\mu - \alpha_e + \sum_i (\beta_{i\mu} \mathcal{C}_{i\mu}^{\text{NP}} - \beta_{ie} \mathcal{C}_{ie}^{\text{NP}}) \\ &+ \sum_{i \geq j} (\gamma_{ij\mu} \mathcal{C}_{i\mu}^{\text{NP}} \mathcal{C}_{j\mu}^{\text{NP}} - \gamma_{ije} \mathcal{C}_{ie}^{\text{NP}} \mathcal{C}_{je}^{\text{NP}}) \end{aligned} \quad (5.4)$$

- LFUV ratios: these type of observables are defined as ratios of integrated branching fractions involving muonic (numerator) and electronic (denominator) final states and we use ( $i, j = 9, 10, 9', 10'$ ):

$$\frac{\mathcal{O}_\mu}{\mathcal{O}_e} = \frac{\alpha_\mu + \sum_i \beta_{i\mu} \mathcal{C}_{i\mu}^{\text{NP}} + \sum_{i \geq j} \gamma_{ij\mu} \mathcal{C}_{i\mu}^{\text{NP}} \mathcal{C}_{j\mu}^{\text{NP}}}{\alpha_e + \sum_i \beta_{ie} \mathcal{C}_{ie}^{\text{NP}} + \sum_{i \geq j} \gamma_{ije} \mathcal{C}_{ie}^{\text{NP}} \mathcal{C}_{je}^{\text{NP}}} \quad (5.5)$$

Not all observables can be parametrised in a fully satisfying way over this grid through such a quadratic approximation. The difference is at most of 0.3 for all observables (central value and uncertainty) over the whole range of scan.  $P_i(B \rightarrow K^* \mu^+ \mu^-)$  observables turn out to be more difficult to fit with a purely quadratic parametrisation, with differences between the approximate parametrisation and the exact values above 0.15 in some parts of the scan range (this could be expected due to their normalisation, leading to rapidly varying functions when the Wilson coefficients are changed). However, even this approximate parametrisation is able to catch a few interesting aspects of the sensitivity to Wilson coefficients.

## 5.2 Observables as conics

Let us start the discussion with the  $b \rightarrow s\mu\mu$  observables, with a quadratic parametrisation that can be seen as a conic in the space of

$$\mathcal{O} = a + (X - X_0)^T \cdot M \cdot (X - X_0) \quad (5.6)$$

The symmetric matrix  $M$  can be diagonalised as  $M = R^T \cdot \Delta \cdot R$  where  $R$  is an orthogonal (rotation) matrix, and  $\Delta$  is a diagonal matrix with eigenvalues ordered in (absolute) size. We can define the (rotated)  $Y$ -basis

$$Y = R \cdot (X - X_0) \quad \mathcal{O} = a + R^T \cdot \Delta \cdot R \quad (5.7)$$

The largest eigenvalues of  $\Delta$  correspond to directions in the  $Y$ -basis that are able to change the value of  $\mathcal{O}$  in the most significant way. These directions correspond to linear combinations of Wilson coefficients to which the observable  $\mathcal{O}$  is the most sensitive.

We can consider the directions corresponding to the largest eigenvalues in absolute value (“dominant ones”) and we can determine whether some directions are similar for different observables. This will indicate that some observables share the same sensitivity to NP for their dominant directions. We perform this comparison considering only the dominant eigenvalue as well as the eigenvalues that are at most 80% of this eigenvalue<sup>5</sup>, and we consider “parallel” directions that correspond to pairs of vectors with an angle with a cosine of 0.9 or more (in absolute value). We perform this comparison for all the bins of the different observables. Due to the large number of directions to consider, we give our conclusions in a compact way, where each observable mentioned means “some of the bins of this observable”. We can observe several classes of observables exhibiting dominant parallel directions:

- observables which are expected to exhibit similar directions due to flavour symmetries

$$\mathcal{B}(B^0 \rightarrow K^{*0}), \mathcal{B}(B^+ \rightarrow K^{*+}), \mathcal{B}(B_s \rightarrow \phi) \quad \mathcal{B}(B^0 \rightarrow K^0), \mathcal{B}(B^+ \rightarrow K^+) \quad (5.8)$$

$$P_i(B^0 \rightarrow K^{*0}), P_i(B_s \rightarrow \phi) \quad (i = 1, 4, 6, F_L) \quad (5.9)$$

---

<sup>5</sup>Let us add that the comparison of eigenvalues can be performed only for a given observable (possibly in different bins). The rescaling of an observable by an arbitrary factor will affect the absolute values of the eigenvalues but not their relative importance.

- observables from the same process

$$\mathcal{B}(B^0 \rightarrow K^{*0}), P_i(B^0 \rightarrow K^{*0}) \quad (i = 1, 3, 4, 5, 6, 8, F_L) \quad (5.10)$$

$$\mathcal{B}(B_s \rightarrow \phi), P_i(B_s \rightarrow \phi) \quad (i = 1, 4, 6, F_L) \quad (5.11)$$

$$P_i(B_s \rightarrow \phi), P_j(B_s \rightarrow \phi) \quad (\{i, j\} = \{F_L, 1\}, \{F_L, 4\}, \{1, 4\}) \quad (5.12)$$

$$P_i(B^0 \rightarrow K^{*0}), P_j(B^0 \rightarrow K^{*0}) \quad (5.13)$$

$$(\{i, j\} = \{F_L, 1\}, \{F_L, 2\}, \{F_L, 4\}, \{F_L, 8\}, \quad (5.14)$$

$$\{1, 2\}, \{1, 3\}, \{1, 4\}, \{1, 5\}, \{1, 8\}, \quad (5.15)$$

$$\{2, 4\}, \{2, 5\}, \{2, 6\}, \{2, 8\}, \{3, 4\}, \{3, 8\}, \{4, 8\}, \{6, 7\}) \quad (5.16)$$

- observables with unexpected correlations

$$\mathcal{B}(B^+ \rightarrow K^+), \mathcal{B}(B^0 \rightarrow K^0), P_1(B^0 \rightarrow K^{*0}), P_1(B_s \rightarrow \phi), P_3(B^0 \rightarrow K^{*0}) \quad (5.17)$$

If we now restrict the analysis to observables that are currently deviating by more than  $2\sigma$ , we can easily consider a wider range of directions in each case (going down to eigenvalues that are 30% of the maximal ones), we can provide a slightly more precise description of the correlations

- between observables as expected from flavour symmetries:

$$\mathcal{B}(B^0 \rightarrow K^{*0})[15, 19], \mathcal{B}(B^+ \rightarrow K^{*+})[15, 19], \mathcal{B}(B_s \rightarrow \phi)[15, 18.8] \quad (5.18)$$

- between different close bins of the same observable

$$P'_5(B^0 \rightarrow K^{*0})[4, 6], P'_5(B^0 \rightarrow K^{*0})[6, 8] \quad (5.19)$$

$$\mathcal{B}(B_s \rightarrow \phi)[2, 5], \mathcal{B}(B_s \rightarrow \phi)[5, 8] \quad (5.20)$$

- between observables that are not obviously correlated

$$\mathcal{B}(B_s \rightarrow \phi)[2, 5], \mathcal{B}(B_s \rightarrow \phi)[5, 8], P'_5(B^0 \rightarrow K^{*0})[4, 6], \quad (5.21)$$

$$\mathcal{B}(B^0 \rightarrow K^{*0})[15, 19], \mathcal{B}(B^+ \rightarrow K^{*+})[15, 19] \quad (5.22)$$

The same analysis carried out for LFUV quantities involves the same correlations, which is to be expected as they involve ratio or differences of the same observables considered in the muon and the electron cases.

Another comment is in order. We have performed our analysis of the directions in the general case where NP is allowed in  $\mathcal{C}_{9,10,9',10'}$  and we have studied the dominant directions for each observable. Scenarios where some of these NP contributions are assumed to be zero correspond to projections of this analysis on specific hyperplanes. Obviously, if directions are similar in the general  $\mathcal{C}_{9,10,9',10'}$  space, they remain similar after projection on a given hyperplane, but the projection can also lead to additional pairs of observables with (projected) dominant directions that are parallel (although they are not parallel when considered in the whole space).

### 5.3 Directions favoured by the anomalies

Up to now, we have considered only the leading directions (corresponding to the main axes of the conics) for the quadratic approximation of the theoretical expression of the  $b \rightarrow s\mu\mu$  observables. This provides information on the sensitivity to specific directions and the fact that some of these directions are common to several observables. However, since we have not compared these predictions to the deviations observed currently, this does not provide information on the specific changes in the Wilson coefficients preferred by the global fit. One can perform a global analysis of the constraints [46], but one can also exploit the above parametrisation to gain some insights to understand better the outcome of the global fit.

This can be done in the following way. As indicated above, we can write a  $b \rightarrow s\mu\mu$  observable in the  $Y$ -space as

$$\mathcal{O} = a + Y^T \cdot \Delta \cdot Y \quad (5.23)$$

where the largest axis of the conic correspond to the 1st coordinate in the  $Y$ -space, with smaller and smaller axes correspond to the 2nd, 3rd... coordinates. Each observable tends to favour a shift in  $Y$  in order to reduce  $\mathcal{O} - \mathcal{O}_{\text{exp}}$  compared to  $\mathcal{O}_{\text{SM}} - \mathcal{O}_{\text{exp}}$ . One can represent this problem as the fact that the conic  $\mathcal{O} = \mathcal{O}_{\text{exp}}$  does not pass through the SM point  $Y_{\text{SM}} = -R \cdot X_0$ . This distance corresponds to the NP shift to perform in some of the Wilson coefficients. In principle, one could chose any NP shift in the Wilson coefficients to go from the SM point to the conic section  $\mathcal{O} = \mathcal{O}_{\text{exp}}$ , but it turns out to be interesting to think in terms of the main axes of the conic section and first to determine the distance between the SM point and the conic section along a given axis  $i$ . This is obtained by

$$\delta Y_j^{(i)} = \pm \delta_{ij} \sqrt{\frac{\mathcal{O}_{\text{exp}} - a - \sum_{k \neq i} Y_{\text{SM},k}^2}{\Delta_i}} \quad (5.24)$$

which corresponds to a NP in the Wilson coefficients  $\delta X^{(i)} = X_0 + R^T \cdot \delta Y^{(i)}$ .

Let us emphasize that this equation does not necessarily have a solution, as it is not necessarily possible to reach the conic section from the SM in all directions (this is easily seen in the case of an ellipsoid, depending on the position of the SM point, inside, outside and close or outside and far away). The above equation illustrates two different aspects of the problem: on the one hand, a large shift in  $\mathcal{O}$  is achieved along the 1st coordinate through a smaller shift in  $Y$  (and thus in the Wilson coefficients) than along higher coordinates, but on the other hand, the distance between the SM point and the conic section might be easier to bridge along higher coordinates than along the first coordinate. The shifts  $\delta Y^{(i)}$  are thus interesting tools to identify the directions preferred by each observable that deviate significantly from the SM.

If we perform this exercise for the observables deviating by more than  $2\sigma$  and keeping only dominant directions (at least 30% of the largest eigenvalue), we obtain the results in Tab. 1. We computed the distances  $\delta Y^{(i)}$  taking into account both experimental and theoretical uncertainties, as indicated in the corresponding table. We also indicate the corresponding directions in terms of  $X$ -coordinates. We show only directions which can accommodate the central value experimentally measured using the parametrisation that we used.

Observable	Direction $i$	$\delta Y^{(i)}$	$X_i$
$P_2(B^0 \rightarrow K^{*0})$ [0.1,0.98]	1	$11.82 \pm 5.89$	(0.01,0.05,0.66,0.75)
$P_2(B^0 \rightarrow K^{*0})$ [0.1,0.98]	2	$4.71 \pm 3.62$	(-0.47,-0.88,0.02,0.04)
$P_2(B^0 \rightarrow K^{*0})$ [0.1,0.98]	4	$7.93 \pm 6.30$	(0.88,-0.47,0.02,-0.00)
$P'_5(B^0 \rightarrow K^{*0})$ [4.0,6.0]	1	$1.83 \pm 0.24$	(0.94,0.22,-0.26,0.02)
$P'_5(B^0 \rightarrow K^{*0})$ [4.0,6.0]	2	$1.96 \pm 0.28$	(-0.29,0.49,-0.57,0.59)
$P'_5(B^0 \rightarrow K^{*0})$ [4.0,6.0]	4	$8.85 \pm 1.82$	(-0.05,-0.63,-0.74,-0.22)
$P'_5(B^0 \rightarrow K^{*0})$ [6.0,8.0]	1	$1.95 \pm 0.32$	(0.87,0.43,-0.22,-0.04)
$P'_5(B^0 \rightarrow K^{*0})$ [6.0,8.0]	2	$1.84 \pm 0.37$	(-0.31,0.40,-0.60,0.62)
$\mathcal{B}(B^0 \rightarrow K^{*0})$ [15.,19.]	2	$0.79 \pm 0.15$	(0.14,-0.69,-0.14,0.70)
$\mathcal{B}(B^+ \rightarrow K^{*+})$ [15.,19.]	2	$1.18 \pm 0.17$	(0.14,-0.69,-0.14,0.70)
$\mathcal{B}(B_s \rightarrow \phi)$ [2.0,5.0]	2	$2.34 \pm 0.63$	(-0.03,-0.70,0.02,0.71)
$\mathcal{B}(B_s \rightarrow \phi)$ [15.,18.8]	2	$0.65 \pm 0.16$	(-0.36,0.60,0.36,-0.62)

**Table 1:** Distance  $\delta Y^{(i)}$  from the SM to the LFD conic  $\mathcal{O} - \mathcal{O}_{\text{exp}}$  following the main axis  $i$  of the conic section. The last column indicates the vector corresponding to the main axis  $i$  in the basis  $X = (\mathcal{C}_{9\mu}, \mathcal{C}_{10\mu}, \mathcal{C}_{9'\mu}, \mathcal{C}_{10'\mu})$ .

We see that

- $P_2$  is affected by large uncertainties that make it difficult to reach definite conclusions
- the 4 branching ratios prefer a single direction, which is essentially along  $\simeq \mathcal{C}_{10\mu} - \mathcal{C}_{10'\mu}$
- the two bins in  $P'_5$  have similar behaviours, with two directions favoured ( $\mathcal{C}_{9\mu}$  with a small  $\mathcal{C}_{10\mu}$  component, or along  $\simeq \mathcal{C}_{10\mu} - \mathcal{C}_{9'\mu} + \mathcal{C}_{10'\mu}$ )

The opposite signs for  $\mathcal{C}_{10'}$  between the branching ratios and the two bins in  $P'_5$  make it difficult to use this specific parameter to improve the agreement of all observables with experiment. A better agreement between theory and data for these observables can thus be reached by performing shifts in  $\mathcal{C}_{9\mu}$  and  $\mathcal{C}_{10\mu}$ . Naturally, this very qualitative argument does not take into account the remaining observables, which are in good agreement with the SM and constrain also the size of the NP shifts in  $\mathcal{C}_{9\mu}$  and  $\mathcal{C}_{10\mu}$ . However it is interesting to see that this rough analysis in terms of favoured directions supports the outcome of the global fit.

A similar analysis can be performed in the case of  $R_K$  and  $R_{K^*}$ , but almost all directions are equally favoured in both muon and electron directions, without shedding further light on the preferences for the global fit.

## 6 Conclusions

Over the last few years, the rare  $b \rightarrow s\ell\ell$  decays have proved particularly interesting, with a large set of deviations from SM expectations. If a first explanation was provided by a large NP contribution to the Wilson coefficient  $\mathcal{C}_{9\mu}$ , the current set of data allows for

several different NP scenarios, which feature large NP contributions violating lepton-flavour universality (affecting  $b \rightarrow s\mu\mu$  but not  $b \rightarrow see$ ) in connection with the measurement of the LFUV ratios  $R_K$  and  $R_{K^*}$ . This does not exhaust the possibilities, and for instance, it is also possible to add NP contributions satisfying lepton-flavour universality (affecting  $b \rightarrow s\mu\mu$  and  $b \rightarrow see$ ) in the same way. With this wealth of possibilities, it is important to understand how current and forthcoming data may favour one scenario over others, so that one can pin down the best NP explanation for the whole set of anomalies observed.

We have first considered some of the current inner tensions of the fits. We highlighted the situation of  $R_{K^*}$  in the lowest bin, the tension between low and large recoils for  $B_s \rightarrow \phi\mu^+\mu^-$ , and a similar issue with  $B \rightarrow K^*\mu^+\mu^-$  angular observables. We then discussed the impact of forthcoming measurements of  $\langle R_K \rangle_{[1,6]}$  and  $\langle Q_5 \rangle_{[1.1,6]}$  to disentangle NP hypotheses. We considered various central values for these two measurements and we assumed some reduction in the experimental uncertainties in order to study how pulls w.r.t. SM and best-fit points would evolve.  $\langle R_K \rangle_{[1,6]}$  alone proves to have only a limited ability to separate the various NP hypotheses:  $\mathcal{C}_{9\mu}^V = -\mathcal{C}_{9'\mu}^V$  is the only hypothesis strongly affected. On the other hand, the combination of  $\langle R_K \rangle_{[1,6]}$  and  $\langle Q_5 \rangle_{[1.1,6]}$  proves much more efficient to separate various favoured hypotheses, either with only LFUV NP contributions or with both LFUV and LFU contributions.

We then considered two different approaches to understand the current structure of the global fit. Firstly, we discussed the pulls associated with individual observables. Their value can be compared under the SM hypothesis and under various NP hypotheses, indicating whether they are easier to accommodate once NP contributions are added. As could be expected, no single hypothesis is clearly preferred: under each hypothesis, some of the observables get larger pulls and others smaller ones. Still, Hyp. II and V, both fulfilling  $\mathcal{C}_{9\mu}^V = -\mathcal{C}_{10\mu}^V$  work slightly better in reducing the pull<sup>obs</sup> of the LFUV observables, compared to the rest of hypotheses considered. On the contrary, Hyp. I is favoured in order to explain  $B \rightarrow K^*\mu^+\mu^-$  angular observables and Hyp. VII is favoured by  $B_s \rightarrow \phi\mu^+\mu^-$  observables. If  $\langle R_K \rangle_{[1,6]}$  and  $\mathcal{B}(B^+ \rightarrow K^+\mu^+\mu^-)$  had central values  $1\sigma$  higher than their actual experimental value, i.e. closer to the SM value, Hyp. I would also be favoured. Finally, our analysis of the pulls points out the need for a better understanding of the low- $q^2$  region for both  $B \rightarrow K$  and  $B \rightarrow K^*$  channels. Secondly, we looked at approximate quadratic parametrisations of the observables with large pulls in the SM. We could then identify directions in the space of Wilson coefficients to which the observables showed a large sensitivity to any shift. Interestingly, the same directions are often favoured by a large set of observables. We also analysed the shifts preferred by the observables showing large tensions with the SM using the same approach of directions.

The overall conclusion of our study is that the current measurements of  $b \rightarrow s\ell\ell$  observables are not enough to disentangle various NP hypotheses: the tensions with the SM do not point towards an unambiguous NP scenario, and several compete at the same level, with only LFUV-NP contributions or combining LFUV and LFU contributions. The forthcoming result on  $\langle R_K \rangle_{[1,6]}$  could prove interesting in confirming (or not) the existence of LFUV NP contributions, but our study shows that in most cases, this update will not help in lifting the degeneracy among the various NP hypotheses. On the other hand, we

have shown that the determination of  $\langle Q_5 \rangle_{[1.1,6]}$  might bring interesting information that would be complementary to the existing observables and that could help significantly in disentangling the various scenarios (depending on the actual measured value). The use of extended data sets, the analyses in different experimental environments and the inclusion of additional observables will all prove particularly important in the coming months in order to cross-check and constrain the dynamics at work in  $b \rightarrow s\ell\ell$  transitions. This will prove essential to identify models of New Physics that could ultimately resolve the anomalies currently observed in the  $b$ -quark sector.

## Acknowledgments

This work received financial support from the grants CICYT-FEDER-FPA 2014-55613-P and FPA 2017-86989-P [JM, SDG, BC, MA], and from Centro de Excelencia Severo Ochoa SEV-2012-0234 [BC]; from the EU Horizon 2020 program from the grants No. 690575, No. 674896 and No. 692194 [SDG]. J.M. acknowledges financial support from the Catalan ICREA Academia Program. The work of P.M. is supported by the Beatriu de Pinós postdoctoral program of the Government of Catalonia’s Secretariat for Universities and Research of the Ministry of Economy and Knowledge of Spain.

## References

- [1] B. Capdevila, A. Crivellin, S. Descotes-Genon, J. Matias and J. Virto, *JHEP* **1801** (2018) 093 [arXiv:1704.05340 [hep-ph]].
- [2] S. Descotes-Genon, L. Hofer, J. Matias and J. Virto, *JHEP* **1606** (2016) 092 [arXiv:1510.04239 [hep-ph]].
- [3] W. Altmannshofer, P. Stangl and D. M. Straub, *Phys. Rev. D* **96** (2017) no.5, 055008 [arXiv:1704.05435 [hep-ph]].
- [4] W. Altmannshofer, C. Niehoff, P. Stangl and D. M. Straub, *Eur. Phys. J. C* **77** (2017) no.6, 377 [arXiv:1703.09189 [hep-ph]].
- [5] G. D’Amico, M. Nardecchia, P. Panci, F. Sannino, A. Strumia, R. Torre and A. Urbano, *JHEP* **1709** (2017) 010 [arXiv:1704.05438 [hep-ph]].
- [6] L. S. Geng, B. Grinstein, S. Jäger, J. Martin Camalich, X. L. Ren and R. X. Shi, *Phys. Rev. D* **96** (2017) no.9, 093006 [arXiv:1704.05446 [hep-ph]].
- [7] A. Arbey, T. Hurth, F. Mahmoudi and S. Neshatpour, *Phys. Rev. D* **98** (2018) no.9, 095027 [arXiv:1806.02791 [hep-ph]].
- [8] M. Ciuchini, A. M. Coutinho, M. Fedele, E. Franco, A. Paul, L. Silvestrini and M. Valli, *Eur. Phys. J. C* **77** (2017) no.10, 688 [arXiv:1704.05447 [hep-ph]].
- [9] G. Hiller and I. Nisandzic, *Phys. Rev. D* **96** (2017) no.3, 035003 [arXiv:1704.05444 [hep-ph]].
- [10] A. K. Alok, B. Bhattacharya, A. Datta, D. Kumar, J. Kumar and D. London, *Phys. Rev. D* **96** (2017) no.9, 095009 [arXiv:1704.07397 [hep-ph]].
- [11] J. Kumar and D. London, arXiv:1901.04516 [hep-ph].

- [12] M. Algueró, B. Capdevila, S. Descotes-Genon, P. Masjuan and J. Matias, arXiv:1809.08447 [hep-ph].
- [13] T. Hurth, F. Mahmoudi, D. Martinez Santos and S. Neshatpour, Phys. Rev. D **96** (2017) no.9, 095034 [arXiv:1705.06274 [hep-ph]].
- [14] B. Capdevila, S. Descotes-Genon, L. Hofer and J. Matias, JHEP **1704** (2017) 016 [arXiv:1701.08672 [hep-ph]].
- [15] S. Wehle *et al.* [Belle Collaboration], Phys. Rev. Lett. **118** (2017) no.11, 111801 [arXiv:1612.05014 [hep-ex]].
- [16] W. Altmannshofer, M. J. Baker, S. Gori, R. Harnik, M. Pospelov, E. Stamou and A. Thamm, JHEP **1803** (2018) 188 [arXiv:1711.07494 [hep-ph]].
- [17] M. Misiak *et al.*, Phys. Rev. Lett. **98** (2007) 022002 [hep-ph/0609232].
- [18] M. Misiak and M. Steinhauser, Nucl. Phys. B **764** (2007) 62 [hep-ph/0609241].
- [19] S. Descotes-Genon, D. Ghosh, J. Matias and M. Ramon, JHEP **1106** (2011) 099 [arXiv:1104.3342 [hep-ph]].
- [20] D. Asner *et al.* [Heavy Flavor Averaging Group], arXiv:1010.1589 [hep-ex].
- [21] R. Aaij *et al.* [LHCb Collaboration], JHEP **1708** (2017) 055 [arXiv:1705.05802 [hep-ex]].
- [22] R. Aaij *et al.* [LHCb Collaboration], JHEP **1611** (2016) 047 Erratum: [JHEP **1704** (2017) 142] [arXiv:1606.04731 [hep-ex]].
- [23] A. Bharucha, D. M. Straub and R. Zwicky, JHEP **1608** (2016) 098 [arXiv:1503.05534 [hep-ph]].
- [24] A. Khodjamirian, T. Mannel, A. A. Pivovarov and Y.-M. Wang, JHEP **1009** (2010) 089 [arXiv:1006.4945 [hep-ph]].
- [25] N. Gubernari, A. Kokulu and D. van Dyk, JHEP **1901** (2019) 150 [arXiv:1811.00983 [hep-ph]].
- [26] C. Bobeth, M. Chrzaszcz, D. van Dyk and J. Virto, Eur. Phys. J. C **78** (2018) no.6, 451 [arXiv:1707.07305 [hep-ph]].
- [27] S. González-Solís and P. Masjuan, Phys. Rev. D **98** (2018) no.3, 034027 [arXiv:1805.11262 [hep-ph]].
- [28] S. Descotes-Genon, J. Matias and J. Virto, Phys. Rev. D **85** (2012) 034010 [arXiv:1111.4882 [hep-ph]].
- [29] K. De Bruyn, R. Fleischer, R. Knegjens, P. Koppenburg, M. Merk and N. Tuning, Phys. Rev. D **86** (2012) 014027 [arXiv:1204.1735 [hep-ph]].
- [30] K. De Bruyn, R. Fleischer, R. Knegjens, M. Merk, M. Schiller and N. Tuning, Nucl. Phys. B **868** (2013) 351 [arXiv:1208.6463 [hep-ph]].
- [31] S. Descotes-Genon and J. Virto, JHEP **1504** (2015) 045 Erratum: [JHEP **1507** (2015) 049] [arXiv:1502.05509 [hep-ph]].
- [32] F. Dettori and D. Guadagnoli, Phys. Lett. B **784** (2018) 96 [arXiv:1804.03591 [hep-ph]].
- [33] R. Aaij *et al.* [LHCb Collaboration], JHEP **1509** (2015) 179 [arXiv:1506.08777 [hep-ex]].
- [34] R. Aaij *et al.* [LHCb Collaboration], JHEP **1506** (2015) 115 Erratum: [JHEP **1809** (2018) 145] [arXiv:1503.07138 [hep-ex]].

- [35] R. Aaij *et al.* [LHCb Collaboration], JHEP **1809** (2018) 146 [arXiv:1808.00264 [hep-ex]].
- [36] Talk by M. Patel at the Instant Workshop on B meson anomalies held at CERN, May 2017 (<https://indico.cern.ch/event/633880/>)
- [37] M. Iwasaki *et al.* [Belle Collaboration], Phys. Rev. D **72** (2005) 092005 [hep-ex/0503044].
- [38] J. P. Lees *et al.* [BaBar Collaboration], Phys. Rev. Lett. **112** (2014) 211802 [arXiv:1312.5364 [hep-ex]].
- [39] R. Aaij *et al.* [LHCb Collaboration], Phys. Rev. Lett. **118** (2017) no.19, 191801 [arXiv:1703.05747 [hep-ex]].
- [40] A. Lenz *et al.*, Phys. Rev. D **83** (2011) 036004 [arXiv:1008.1593 [hep-ph]].
- [41] J. Charles *et al.*, Phys. Rev. D **84** (2011) 033005 [arXiv:1106.4041 [hep-ph]].
- [42] A. Lenz, U. Nierste, J. Charles, S. Descotes-Genon, H. Lacker, S. Monteil, V. Niess and S. T’Jampens, Phys. Rev. D **86** (2012) 033008 [arXiv:1203.0238 [hep-ph]].
- [43] J. Charles, S. Descotes-Genon, V. Niess and L. Vale Silva, Eur. Phys. J. C **77** (2017) no.4, 214 [arXiv:1611.04768 [hep-ph]].
- [44] [ALEPH and DELPHI and L3 and OPAL and SLD and LEP Electroweak Working Group and SLD Electroweak Group and SLD Heavy Flavour Group Collaborations], Phys. Rept. **427** (2006) 257 [hep-ex/0509008].
- [45] L. Demortier and L. Lyons, *Everything you always wanted to know about pulls*, CDF Note 5776.
- [46] B. Capdevila, U. Laa and G. Valencia, arXiv:1811.10793 [hep-ph].
- [47] J. Matias, F. Mescia, M. Ramon and J. Virto, JHEP **1204** (2012) 104 [arXiv:1202.4266 [hep-ph]].
- [48] W. Altmannshofer, P. Ball, A. Bharucha, A. J. Buras, D. M. Straub and M. Wick, JHEP **0901** (2009) 019 [arXiv:0811.1214 [hep-ph]].
- [49] B. Capdevila, S. Descotes-Genon, J. Matias and J. Virto, JHEP **1610** (2016) 075 [arXiv:1605.03156 [hep-ph]].